Available online at www.sciencedirect.com
ScienceDirect
Geochimica et Cosmochimica Acta 71 (2007) 3717–3745
Geochimica et Cosmochimica Acta
www.elsevier.com/locate/gca

# A predictive model (ETLM) for arsenate adsorption and surface speciation on oxides consistent with spectroscopic and theoretical molecular evidence

Keisuke Fukushi [1], Dimitri A. Sverjensky *

*Department of Earth and Planetary Sciences, Johns Hopkins University, Baltimore, MD 21218, USA*

Received 7 September 2006; accepted in revised form 9 May 2007; available online 7 June 2007

**Abstract**

The nature of adsorbed arsenate species for a wide range of minerals and environmental conditions is fundamental to prediction of the migration and long-term fate of arsenate in natural environments. Spectroscopic experiments and theoretical calculations have demonstrated the potential importance of a variety of arsenate surface species on several iron and aluminum oxides. However, integration of the results of these studies with surface complexation models and extrapolation over wide ranges of conditions and for many oxides remains a challenge. In the present study, *in situ* X-ray and infrared spectroscopic and theoretical molecular evidence of arsenate (and the analogous phosphate) surface speciation are integrated with an extended triple layer model (ETLM) of surface complexation, which takes into account the electrostatic work associated with the ions and the water dipoles involved in inner-sphere surface complexation by the ligand exchange mechanism.

Three reactions forming inner-sphere arsenate surface species

$$2 > \mathrm{SOH} + \mathrm{H_3AsO_4}^0 = (> \mathrm{SO})_2\mathrm{AsO_2}^- + \mathrm{H}^+ + 2\mathrm{H_2O}$$

$$2 > \mathrm{SOH} + \mathrm{H_3AsO_4}^0 = (> \mathrm{SO})_2\mathrm{AsOOH} + 2\mathrm{H_2O}$$

and

$$> \mathrm{SOH} + \mathrm{H_3AsO_4}^0 = > \mathrm{SOAsO_2}^{2-} + 2\mathrm{H}^+ + \mathrm{H_2O}$$

were found to be consistent with adsorption envelope, adsorption isotherm, proton surface titration and proton coadsorption of arsenate on hydrous ferric oxide (HFO), ferrihydrite, four goethites, amorphous aluminum oxide, α-$Al_2O_3$, β-$Al(OH)_3$, and α-$Al(OH)_3$ up to surface coverages of about 2.5 μmol $m^{-2}$. At higher surface coverages, adsorption is not the predominant mode of arsenate sorption. The four goethites showed a spectrum of model arsenate surface speciation behavior from predominantly binuclear to mononuclear. Goethite in the middle of this spectrum of behavior (selected as a model goethite) showed predicted changes in arsenate surface speciation with changes in pH, ionic strength and surface coverage very closely consistent with qualitative trends inferred in published *in situ* X-ray and infrared spectroscopic studies of arsenate and phosphate on several additional goethites. The model speciation results for arsenate on HFO, α- and β-$Al(OH)_3$ were also consistent with X-ray and molecular evidence.

The equilibrium constants for arsenate adsorption expressed in terms of site-occupancy standard states show systematic differences for different solids, including the model goethite. The differences can be explained with the aid of Born solvation theory, which enables the development of a set of predictive equations for arsenate adsorption equilibrium constants on all oxides. The predictive equations indicate that the Born solvation effect for mononuclear species is much stronger than for binuclear species. This favors the development of the mononuclear species on iron oxides such as HFO with high values of the dielectric constant relative to aluminum oxides such as gibbsite with much lower dielectric constants. However, on

* Corresponding author. Fax: +1 410 516 7933.
*E-mail addresses:* fukushi@kenroku.kanazawa-u.ac.jp (K. Fukushi), sver@jhu.edu (D.A. Sverjensky).
[1] Present address: Institute of Nature and Environmental Technology, Kanazawa University, Kakuma-machi, Kanazawa, Ishikawa 920-1192, Japan.

0016-7037/$ - see front matter 
doi:10.1016/j.gca.2007.05.018

hematite and corundum, with similar dielectric constants, the predicted surface speciations of arsenate are similar: at lower pH values and/or higher surface coverages, binuclear species are predicted to predominate, at higher pH values and/or lower surface coverages, mononuclear species predominate.


## 1. INTRODUCTION

Arsenic has received a great deal of public attention because of its links to certain types of cancers and its high levels in some drinking water supplies (Nordstrom, 2002; Hopenhayn, 2006). Arsenate is the predominant species of arsenic in oxidized aquatic systems (Myneni et al., 1998). The concentration of arsenate in natural waters is strongly influenced by adsorption on oxide surfaces (Fuller and Davis, 1989; Pichler et al., 1999; Fukushi et al., 2003). To predict the migration and long-term fate of arsenate in natural environments, the behavior and the nature of adsorbed arsenate species must be known for a wide variety of minerals and over the full range of environmental conditions.

The surface speciation of arsenate on oxide powders and on single crystal surfaces has been studied through X-ray spectroscopic and infrared investigations as well as theoretical molecular calculations. On powders, a variety of surface species have been inferred from extended X-ray absorption fine structure (EXAFS) studies. The majority of these studies have been concerned with iron oxides and a very limited range of ionic strengths. For arsenate on ferrihydrite and FeOOH polymorphs (goethite, akaganeite and lepidocrocite) at pH 8 and $I = 0.1$, it was inferred that arsenate adsorbed mainly as an inner-sphere bidentate-binuclear complex (Waychunas et al., 1993). Monodentate-mononuclear complexes were also inferred. The monodentate/bidentate ratio decreased with increasing arsenate surface coverage. In contrast, Manceau (1995) reinterpreted the EXAFS spectra as indicating bidentate-mononuclear species. The possible existence of such a species, in addition to the ones described by Waychunas et al. (1993) was described in Waychunas et al. (2005).

All three of the above species were subsequently inferred for arsenate adsorption on goethite from EXAFS results obtained at pH 6–9 and $I = 0.1$ (Fendorf et al., 1997).The monodentate-mononuclear species was inferred to dominate at higher pH values and lower surface coverages, whereas the bidentate-binuclear species dominated at lower pH and higher surface coverages. The bidentate-mononuclear species was detected in only minor amounts at high surface coverage. For arsenate on goethite and lepidocrocite at pH 6, a bidentate-binuclear species was inferred (Farquhar et al., 2002). The same species was inferred for arsenate on goethite, lepidocrocite, hematite and ferrihydrite at pH 4 and 7 and $I = 0.1$ through EXAFS combined with molecular calculations (Sherman and Randall, 2003). For arsenate on hematite, as a function of pH 4.5–8 and surface coverage, Arai et al. (2004) interpreted EXAFS data to infer a predominant bidentate-binuclear and a minor amount of a bidentate-mononuclear species. In the only powder studies of aluminum oxides, EXAFS and XANES of arsenate adsorption on β-$Al(OH)_3$ at pH 4, 8, and 10 and $I = 0.1$ and 0.8 by Arai et al. (2001) showed that arsenate adsorbs to β-$Al(OH)_3$ as a bidentate-binuclear inner-sphere species (their XANES data did not indicate any outer-sphere species regardless of pH and ionic strength), and an EXAFS study of arsenate on α-$Al(OH)_3$ at pH 5.5 (in dilute Na-arsenate solutions) also showed that arsenate forms an inner-sphere bidentate-binuclear species (Ladeira et al., 2001).

On single crystal surfaces of corundum and hematite, several arsenate surface species have been reported recently. For the (0 0 0 1) and (10–12) planes of hematite, prepared at pH 5 with $10^{-4}$ M sodium arsenate solutions, then studied with GIXAFS and surface diffraction in a humid atmosphere, 71–78% of the adsorbed arsenate was determined to be a bidentate-mononuclear species, with the remainder present as a bidentate-binuclear species (Waychunas et al., 2005). However, in bulk water at pH 5, resonant anomalous X-ray reflectivity and standing-wave studies of the (01–12) planes of corundum and hematite, have established a bidentate-binuclear species, and the first reported occurrence of an outer-sphere or H-bonded arsenate species (Catalano et al., 2006a,b; 2007). In the present study, we wish to emphasize that distinguishing between an outer-sphere and H-bonded species is not possible in surface complexation models of reaction stoichiometry, although considerations of Born solvation theory may facilitate the distinction.

Overall, the X-ray studies on powders and single crystals provide strong indications of a variety of surface arsenate species, presumably present under different conditions of pH, ionic strength and surface coverage, as well as being present on different solids and crystallographically different surfaces. Even on a single crystal surface, a great variety of possible surface species coordination geometries can be proposed, e.g. monodentate, bidentate and tridentate possibilities (Waychunas et al., 2005). However, the most frequently reported inner-sphere arsenate species coordination geometries in X-ray studies remain the bidentate-binuclear, bidendate-mononuclear, and the monodentate-mononuclear types of species. In this regard, it should also be emphasized that none of the protonation states of these coordination geometries are established by X-ray studies. A variety of possible protonation states adds even further potential complexity to the speciation of adsorbed arsenate. It is here that other spectroscopic techniques (e.g. infrared and Raman) and molecular calculations, as well as the reaction stoichiometries in surface complexation models can possibly help.

*In situ* ATR-FTIR studies of arsenate on ferrihydrite and amorphous hydrous ferric hydroxide have inferred that adsorption of arsenate occurred as inner-sphere species (Roddick-Lanzilotta et al., 2002; Voegelin and Hug, 2003). An *ex situ* FTIR study (Sun and Doner, 1996) has

inferred binuclear-bridging complexes of arsenate on goethite. However, the latter noted that their results could be affected by not having bulk water present in their spectroscopic experiment. In addition, IR studies of arsenate adsorption may only show small or no shifts with changes of pH (Goldberg and Johnston, 2001). As a consequence, the assignment of arsenate surface species from infrared and Raman spectra is sufficiently difficult (Myneni et al., 1998) that a definitive *in situ* study has yet to be done. Consequently, in the present study we have made use of *in situ* infrared results for an analogous anion phosphate.

Phosphate and arsenate have very similar aqueous protonation characteristics and are widely considered to have very similar adsorption characteristics (Waychunas et al., 1993; Hiemstra and van Riemsdijk, 1999; Goldberg and Johnston, 2001; Arai et al., 2004). Furthermore, infrared studies of phosphate adsorption indicate enough shifts of the spectra with experimental conditions to assign the phosphate surface species (Tejedor-Tejedor and Anderson, 1990; Persson et al., 1996; Arai and Sparks, 2001; Loring et al., 2006; Nelson et al., 2006). The phosphate surface species inferred by Tejedor-Tejedor and Anderson (1990) have already been used to develop a CD surface complexation model for arsenate on goethite (Hiemstra and van Riemsdijk, 1999). In the present study, we take a similar approach using the studies by Tejedor-Tejedor and Anderson (1990), Arai and Sparks (2001), and Elzinga and Sparks (2007) which are the definitive published studies of phosphate adsorption referring to *in situ* conditions. It should be emphasized here that, in detail, there are differences between some of the surface species inferred in the above studies. In the present study, we investigated a surface complexation application of the species suggested by these authors to see if a consistent set of species would apply to a wide range of oxides.

According to Tejedor-Tejedor and Anderson (1990), phosphate on goethite adopts three surface species: protonated bidentate-binuclear, deprotonated bidentate-binuclear and deprotonated monodentate species. The relative abundances of these species were shown to be strong functions of pH and surface coverage at an ionic strength of 0.01. The protonated bidentate-binuclear species predominated at pH values of about 3.6 to 5.5–6.0 (at surface coverages of 190 and 150 μmol/g). The deprotonated bidentate-binuclear species became predominant between pH values of about 6–8.3. The mondentate species was detectable at pH values as low as 6 at surface coverages of 190 μmol/g and increased in relative abundance as the surface coverage decreased towards 50 μmol/g. Consistent results have been obtained for phosphate on ferrihydrite (Arai and Sparks, 2001). The latter assigned protonated bidentate-binuclear species at pH values of 4 to 6 and surface coverages of 0.38–2.69 μmol/$m^2$ and a deprotonated bidentate-binuclear species at pH >7.5, as well as a possible non-protonated Na-phosphate surface species at high pH values. More recently, in an investigation of phosphate adsorption on hematite, Elzinga and Sparks (2007) suggested a bridging binuclear protonated species, a protonated mononuclear species and a deprotonated mononuclear species. It was also suggested that the "bridging" species may instead be mononuclear with a strong H-bond to an adjacent Fe-octahedra. Broadly speaking, the *in situ* infrared studies for phosphate adsorption on iron oxides are consistent with the results of the X-ray studies for arsenate discussed above (although the X-ray studies cannot provide information on protonation states). However, the above infrared studies of phosphate provide invaluable additional information on the possible states of protonation of the surface phosphate species, which we use as a first step in developing a surface complexation model for arsenate adsorption below.

The surface structure and protonation state of adsorbed arsenate have been addressed through theoretical density functional theory (DFT) and molecular orbital density functional theory (MO/DFT) calculations (Ladeira et al., 2001; Sherman and Randall, 2003; Kubicki, 2005). DFT calculations for arsenate with aluminum oxide clusters indicated that a bidentate-binuclear species was more stable than bidentate-mononuclear, monodentate-mononuclear or monodentate-binuclear species (Ladeira et al., 2001). From predicted geometries of arsenate adsorbed on iron hydroxide clusters using DFT comparing EXAFS data, it was suggested that arsenate was adsorbed as a doubly protonated species (Sherman and Randall, 2003). Predicted energetics indicated that a bidentate-binuclear species was more stable than a bidentate-mononuclear and monodentate species. In contrast to these DFT calculations, MO/DFT calculations by using a different type of iron hydroxide clusters (containing solvated waters) showed that deprotonated arsenate surface species resulted in good agreement with spectroscopic data (Kubicki, 2005). The bidentate-binuclear configuration is most consistent with spectroscopic data, but the model Gibbs free energies of adsorption of clusters suggested that the monodentate configuration is energetically more stable as a cluster. The MO/DFT calculations also indicated a strong preference for arsenate to bind to iron clusters relative to aluminum hydroxide clusters. Detailed molecular simulations of phosphate on iron oxide clusters (Kwon and Kubicki, 2004) emphasize mononuclear species with differing protonation states that agree very well with an *ex situ* infrared study of phosphate on goethite (Persson et al., 1996).

Numerous studies have focused on surface complexation modeling of arsenate on oxides (Goldberg, 1986; Dzombak and Morel, 1990; Manning and Goldberg, 1996; Grossl et al., 1997; Manning and Goldberg, 1997; Hiemstra and van Riemsdijk, 1999; Gao and Mucci, 2001; Goldberg and Johnston, 2001; Halter and Pfeifer, 2001; Dixit and Hering, 2003; Arai et al., 2004; Hering and Dixit, 2005). Surface complexation modeling has the capability to predict the behavior and the nature of adsorbed arsenate species as functions of environmental parameters. However, the complexation reactions have not always been consistent with *in situ* spectroscopic results. Instead, with the exception of the study by Hiemstra and van Riemsdijk (1999), regression of macroscopic adsorption data has often been carried out merely to fit the data with the minimum number of surface species (Hering and Dixit, 2005). It is now widely recognized that the evidence of oxyanion speciation from spectroscopic studies should be integrated with models describing macroscopic adsorption and

electrokinetic data (Suarez et al., 1997; Hiemstra and van Riemsdijk, 1999; Blesa et al., 2000; Goldberg and Johnston, 2001).

In the present study, we use the results of the *in situ* X-ray and infrared studies of arsenate and phosphate discussed above to guide the choice of surface species in the extended triple-layer model (ETLM) recently developed to account for the electrostatic effects of water-dipole desorption during inner-sphere surface complexation (Sverjensky and Fuksuhi, 2006a,b). We investigate the applicability of three spectroscopically identified species by fitting adsorption, proton surface titration in the presence of arsenate, and proton coadsorption with arsenate on a wide range of oxides including goethite, hydrous ferric oxide (HFO), ferrihydrite, hematite, amorphous aluminum oxide, β-$Al(OH)_3$, α-$Al(OH)_3$ and α-$Al_2O_3$ (Manning and Goldberg, 1996; Jain et al., 1999; Jain and Loeppert, 2000; Arai et al., 2001, 2004; Gao and Mucci, 2001; Goldberg and Johnston, 2001; Halter and Pfeifer, 2001; Dixit and Hering, 2003). These data were selected to cover wide ranges of pH, ionic strength and surface coverage, and a wider range of oxide types than have been investigated spectroscopically. Other arsenate data examined in the present study (Rietra et al., 1999; Arai et al., 2004; Dutta et al., 2004; Pena et al., 2005, 2006; Zhang and Stanforth, 2005) did not involve a wide enough range of conditions to permit retrieval of equilibrium constants for three surface species. Electrokinetic data involving arsenate adsorption were also examined in the present study (e.g. Anderson and Malotky, 1979; Arai et al., 2001; Goldberg and Johnston, 2001; Pena et al., 2006). However, these data refer to a much more limited range of conditions.

The main purpose of the present study is to determine the effects of pH, ionic strength, surface coverage and type of solid on the surface speciation of arsenate identified spectroscopically. The results are then compared with independent trends established in X-ray and infrared spectroscopic studies for arsenate and phosphate. A second goal of the present study is to provide a predictive basis for arsenate surface speciation on all oxides. By adopting an internally consistent set of standard states, systematic differences in the equilibrium constants for the surface arsenate species from one oxide to another can be established and explained with the aid of Born solvation theory. This makes it possible to predict arsenate adsorption and surface speciation on all oxides in 1:1 electrolyte systems.

## 2. ETLM TREATMENT OF ARSENATE ADSORPTION

### 2.1. Aqueous speciation, surface protonation and electrolyte adsorption

Aqueous speciation calculations were carried out taking into account aqueous ionic activity coefficients appropriate to single electrolytes up to high ionic strengths calculated with the extended Debye-Huckel equation (Helgeson et al., 1981; Criscenti and Sverjensky, 1999). Electrolyte ion pairs used were consistent with previous studies (Criscenti and Sverjensky, 1999, 2002). Aqueous arsenate protonation equilibria were taken from a recent study (Nordstrom and Archer, 2003):

$$H^+ + H_2AsO_4^- = H_3AsO_4^0; \quad \log K = 2.30 \tag{1}$$

$$H^+ + HAsO_4^{2-} = H_2AsO_4^-; \quad \log K = 6.99 \tag{2}$$

$$H^+ + AsO_4^{3-} = HAsO_4^{2-}; \quad \log K = 11.8 \tag{3}$$

Aqueous arsenate complexation with the electrolyte cations used in experimental studies can be expected to occur, based on the analogous phosphate systems. However, the lack of experimental characterization of arsenate-electrolyte cation complexing prevented including this in the present study. Preliminary calculations carried out using Na-complexes of phosphate as a guide to the strength of Na–arsenate complexes indicated that the results of the present study were not significantly affected at ionic strengths of 0.1 and below.

The sample characteristics and surface protonation and electrolyte adsorption equilibrium constants used in the present study are summarized in Table 1. Although HFO and ferrihydrite might be thought to have extremely similar surface chemical properties, we distinguished between them in our previous study of As(III) adsorption (Sverjensky and Fukushi, 2006b). By using differences in the $pH_{ZPC}$ (i.e. 7.9 vs. 8.5, respectively, Table 1), we inferred different effective dielectric constants for these solids, which facilitated the use of Born solvation theory to explain the different magnitudes of the $\log K$ values for As(III) adsorption. It will be shown below that the same approach works for differences in arsenate adsorption, at least for these specific HFO and ferrihydrite samples. Surface protonation constants referring to the site-occupancy standard states (denoted by the superscript "$\theta$"), i.e. $\log K_1^\theta$ and $\log K_2^\theta$, were calculated from values of $pH_{ZPC}$ and $\Delta pK_n^\theta$ (Sverjensky, 2005) using

$$\log K_1^\theta = pH_{ZPC} - \frac{\Delta pK_n^\theta}{2} \tag{4}$$

and

$$\log K_2^\theta = pH_{ZPC} + \frac{\Delta pK_n^\theta}{2} \tag{5}$$

Values of $pH_{ZPC}$ were taken from measured low ionic strength isoelectric points or point-of-zero-salt effects corrected for electrolyte adsorption (Sverjensky, 2005). For goethite and HFO examined by Dixit and Hering (2003), neither isoelectric points nor surface titration data were reported. The value of $pH_{ZPC}$ for the goethite was predicted for the present study using Born solvation and crystal chemical theory (Sverjensky, 2005). For HFO, the $pH_{ZPC}$ was assumed to be the same as in Davis and Leckie (1978), consistent with our previous analysis for arsenite adsorption on the same sample of HFO (Sverjensky and Fukushi, 2006). Values of $\Delta pK_n^\theta$ were predicted theoretically (Sverjensky, 2005).

For convenience, protonation constants referring to the hypothetical 1.0 molar standard state (denoted by the superscript "0") are also given in Table 1. The relationship between the two standard states is given by (Sverjensky, 2003)

Table 1
Sample characteristics, surface protonation and electrolyte adsorption equilibrium constants, and capacitances used in the present study

| Solid | Salt (ML) | $N_s$[a] ($nm^{-1}$) | $A_s$[b] ($m^2\ g^{-1}$) | $pH_{ZPC}$[c] | $\Delta pK_1^{\theta}$[d] | $\log K_1^{\theta}$ | $\log K_2^{\theta}$ | $\log K_1^0$ | $\log K_2^0$ | $\log K_M^{\theta}$ | $\log K_L^{\theta}$ | $\log {}^*K_M^0$ | $\log {}^*K_L^0$ | $C_1$ ($\mu F\ cm^2$) | Adsorption data |
|---|---|---|---|---|---|---|---|---|---|---|---|---|---|---|---|
| HFO | $NaClO_4$ | 3.8 | 600 | 7.9 | 5.6 | 5.1 | 10.7 | 3.7 | −12.1 | 4.3[e] | 4.5[e] | −7.8 | 8.2 | 100[e] | Dixit and Hering (2003) |
| Ferrihydrite | NaCl | 3.8 | 600 | 8.5 | 5.6 | 5.7 | 11.3 | 4.3 | −12.7 | 4.0[f] | 4.0[f] | −8.7 | 8.3 | 110[f] | Jain et al. (1999, 2000) |
| Goethite | $NaClO_4$ | 3.5 | 54 | 9.2 | 5.6 | 6.4 | 12.0 | 6.1 | −12.3 | 3.4 | 2.4 | −8.9 | 8.5 | 120 | Dixit and Hering (2003) |
| Goethite | NaCl | 4.5 | 27.7 | 8.5 | 5.6 | 5.6 | 11.4 | 5.5 | −11.5 | 2.4[g] | 2.3[g] | −9.0 | 7.9 | 120[g] | Gao and Mucci (2001) |
| Goethite | $KNO_3$ | 3.5 | 70.8 | 9.3 | 5.6 | 6.5 | 12.1 | 6.1 | −12.5 | 2.7[g] | 2.6[g] | −9.8 | 8.7 | 100[g] | Antelo et al. (2005) |
| Goethite | NaCl | 3.9 | 43.7 | 8.7 | 5.6 | 5.9 | 11.5 | 5.7 | −11.7 | 3.4 | 3.2 | −8.3 | 8.9 | 140 | Manning and Goldberg (1996) |
| α-$Al_2O_3$ | $NaNO_3$ | 3.0 | 10.9 | 9.2 | 5.6 | 6.4 | 12.0 | 6.9 | −11.5 | 2.6[g] | 2.4[g] | −8.9 | 9.3 | 105[g] | Halter and Pfeifer (2001) |
| β-$Al(OH)_3$ | $NaNO_3$ | 5.0 | 90.1 | 9.3 | 5.6 | 6.5 | 12.1 | 5.8 | −12.8 | 2.9[h] | 2.7[h] | −9.9 | 8.5 | 60[h] | Arai et al. (2001) |
| am·AlO | NaCl | 2.5 | 600 | 9.4 | 5.6 | 6.6 | 12.2 | 5.4 | −13.4 | 3.1[h] | 2.7[h] | −10.3 | 8.1 | 160[h] | Goldberg and Johnston (2001) |
| α-$Al(OH)_3$ | NaCl | 3.0 | 45 | 9.8 | 5.6 | 7.0 | 12.6 | 6.9 | −12.7 | 2.9 | 2.4 | −9.8 | 9.3 | 60 | Manning and Goldberg (1996) |

Values of $\log K_1^{\theta}$, $\log K_2^{\theta}$, $\log K_{M^+}^{\theta}$ and $\log K_{L^-}^{\theta}$ refer to site-occupancy standard states for the reactions ($\log K_1^{\theta}$ :> $SOH + H^+ => SOH_2^+$; $\log K_2^{\theta}$ :> $SO^- + H^+ => SOH$; $\log K_{M^+}^{\theta}$ :> $SO^-$ + $M^+ => SO^-$–$M^+$; $\log K_{L^-}^{\theta}$ :> $SOH_2^+ + L^- => SOH_2^+$–$L^-$). Values of $\log K_1^{\theta}$ and $\log K_2^{\theta}$ were predicted using the given values of $pH_{ZPC}$ and $\Delta pK_n^{\theta}$. Values of $\log K_{M^+}^{\theta}$, $\log K_{L^-}^{\theta}$ and $C_1$ were taken from published theoretical predictions (Sverjensky, 2005) unless otherwise noted. Values for $\log {}^*K_2^0$, $\log {}^*K_{M^+}^0$ and $\log {}^*K_{L^-}^0$ refer to the hypothetical 1.0 M standard state and the reactions ($\log {}^*K_1^0$ :> $SOH + H^+ => SOH_2^+$; $\log {}^*K_2^0$ :> $SO^- + H^+ => SOH$; $\log {}^*K_{M^+}^0$ :> $SOH + M^+ => SO^-$–$M^+ + H^+$; $\log {}^*K_{L^-}^0$ :> $SOH + H^+ + L^- => SOH_2^+$–$L^-$). They were calculated from the values of $\log K_1^{\theta}$, $\log K_2^{\theta}$, $\log K_{M^+}^{\theta}$ and $\log K_{L^-}^{\theta}$ with the aid of Eqs. (6)–(9) using the tabulated values of $N_S$, $A_S$, $pH_{ZPC}$ and $\Delta pK_n^{\theta}$.

[a] Values generated by regression of arsenate adsorption as a function of surface coverage, with the following exceptions: values for HFO, ferrihydrite, β-$Al(OH)_3$, FeOOH (Dixit and Hering, 2003) and am·AlO were taken from previous regression calculations of arsenite adsorption data on the same samples (Sverjensky and Fukushi, 2006b); the value for the Manning and Goldberg goethite was generated with the equation for the line in Fig. 6 based on arsenite and sulfate regressions (Fukushi and Sverjensky, 2006).

[b] Surface areas from BET measurements by the authors listed with the exception of HFO (Dixit and Hering, 2003), ferrihydrite (Jain et al., 2001) and am·AlO (Goldberg and Johnston, 2001) for which the surface area was taken from the study of hydrous ferric hydroxide by Davis and Leckie (1978).

[c] Zero points of charge taken from measured low ionic strength isoelectric points for FeOOH (Manning and Goldberg, 1996), β-$Al(OH)_3$ (Arai et al., 2001), am·AlO (Goldberg and Johnston, 2001) and α-$Al(OH)_3$ (Manning and Goldberg, 1996). The value for FeOOH (Dixit and Hering, 2003) was predicted theoretically (Sverjensky, 2005). Value for hematite (Arai et al., 2001) is taken from low ZPC hematite (Sverjensky, 2005). Values for ferrihydrite (Jain et al., 1999 and Jain and Loeppert, 2000), FeOOH (Gao and Mucci, 2001) and α-$Al_2O_3$ (Halter and Pfeifer, 2001) represent values of $pH_{PZSE}$ from titration data by Jain et al. (1999); Gao and Mucci (2001) and Halter (1999), respectively, corrected for electrolyte effects after Sverjensky (2005). The value for HFO (Dixit and Hering, 2003) was assumed to be the same as measured by Davis and Leckie (1978).

[d] Predicted theoretically (Sverjensky, 2005).

[e] Calculated from the results of regression by Criscenti and Sverjensky (2002) of HFO proton surface charge data from Davis and Leckie (1978).

[f] Calculated from the resuts of regression by Sverjensky and Fukushi (2006b) of ferrihydrite proton surface charge data from Jain et al. (1999).

[g] Calculated from the results of regression of proton surface charge data in the present study (Figs. 3a, 5a and 11a).

[h] Taken from Sverjensky and Fukushi (2006b).

$$\log K_1^0 = \log K_1^\theta - \log\left(\frac{N_S A_S}{N^\ddagger A^\ddagger}\right) \quad (6)$$

$$\log K_2^0 = \log K_2^\theta + \log\left(\frac{N_S A_S}{N^\ddagger A^\ddagger}\right) \quad (7)$$

where, $N_S$ represents the surface site density on the $s$th solid sorbent (sites $m^{-2}$); $N^\ddagger$ represents the standard state sorbate species site density (sites $m^{-2}$); $A_S$ represents the BET surface area of the $s$th solid sorbent ($m^2\ g^{-1}$); $A^\ddagger$ represents a standard state BET surface area ($m^2\ g^{-1}$).

In the present study, values of $N^\ddagger = 10 \times 10^{18}$ sites $m^{-2}$ and $A^\ddagger = 10\ m^2\ g^{-1}$ are selected for all solids.

Electrolyte adsorption equilibrium constants referring to site-occupancy standard states, $\log K^\theta_{M^+}$ and $\log K^\theta_{L^-}$, and capacitances, $C_1$, were obtained from regression of proton surface charge data when such data were available. Otherwise, these parameters were obtained from theoretical predictions (Sverjensky, 2005). For convenience, Table 1 also contains values of the electrolyte adsorption equilibrium constants relative to the >SOH species (denoted by the superscript "*") and with respect to the hypothetical 1.0 molar standard state, i.e. $\log {}^*K^0_{M^+}$ and $\log {}^*K^0_{L^-}$. The relationships of $\log {}^*K^0_{M^+}$ and $\log {}^*K^0_{L^-}$ to $\log K^\theta_{M^+}$ and $\log K^\theta_{L^-}$ are given by (Sverjensky, 2003, 2005)

$$\log {}^*K^0_{M^+} = \log K^\theta_{M^+} - pH_{ZPC} - \frac{\Delta pK^\theta_n}{2} - \log\left(\frac{N_S A_S}{N^\ddagger A^\ddagger}\right) \quad (8)$$

$$\log {}^*K^0_{L^-} = \log K^\theta_{L^-} + pH_{ZPC} - \frac{\Delta pK^\theta_n}{2} - \log\left(\frac{N_S A_S}{N^\ddagger A^\ddagger}\right) \quad (9)$$

Surface areas ($A_S$) were taken from experimental measurements (BET) for goethite, α-$Al(OH)_3$, β-$Al(OH)_3$ and α-$Al_2O_3$. However, for samples of HFO, ferrihydrite and am·AlO, it was assumed that the surface areas are $600\ m^2.g^{-1}$ consistent with recommendations made previously (Davis and Leckie, 1978; Dzombak and Morel, 1990) and our previous analyses of arsenite and sulfate adsorption on these oxides.

Site densities ($N_S$) together with arsenate adsorption equilibrium constants were derived from regression of adsorption data where these data referred to a wide enough range of surface coverages. This procedure was adopted because oxyanions probably form inner-sphere complexes on only a subset of the total sites available, most likely the singly coordinated oxygens at the surface (Catalano et al., 2006a,b,c,d; 2007; Hiemstra and van Riemsdijk, 1999). Theoretical estimation of these site densities is impossible for powdered samples when the proportions of the crystal faces are unknown, as is the case for all the experimental studies analyzed below. Furthermore, for goethites, surface chemical characteristics vary widely, even for those synthesized in the absence of $CO_2$ (Sverjensky, 2005). Together with site densities for goethites already published (Sverjensky and Fukushi, 2006a,b), the goethite site densities obtained by regression in the present study, with one exception, support an empirical correlation between site density and surface area of goethite (Fukushi and Sverjensky, 2007). This correlation should enable estimation of site densities for those goethites for which oxyanion adsorption data over a wide range of surface coverage are not available. In the cases of arsenate adsorption on HFO, ferrihydrite, goethite from Dixit and Hering (2003), and β-$Al(OH)_3$ and am·AlO, the site densities were taken from our previous regression of arsenite adsorption data (Sverjensky and Fukushi, 2006b). We used a single site density for each sample applied to all the surface equilibria as described previously (Sverjensky and Fukushi, 2006b). All the calculations were carried out with the aid of the computer code GEOSURF (Sahai and Sverjensky, 1998).

### 2.2. Arsenate adsorption reaction stoichiometries

We constructed our ETLM for arsenate adsorption on oxides by choosing surface species based on the *in situ* X-ray and infrared spectroscopic studies of phosphate and arsenate and the molecular calculations for arsenate interaction with metal oxide clusters. We used three reaction stoichiometries expressed as the formation of inner-sphere surface species as illustrated in Fig. 1. Additional species could be incorporated into the model, but even the data analyzed in the present study, which refers to a wide range of experimental conditions, did not permit retrieval of equilibrium constants for more than three surface species. We tested numerous reaction stoichiometries, but found that the best three reaction stoichiometries involved surface species identical to the ones proposed in the *in situ* ATR-FTIR study of phosphate adsorption on goethite (Tejedor-Tejedor and Anderson, 1990) discussed above. For the most part, these species are also consistent with the X-ray studies cited above.

The three reactions produce a deprotonated bidentate-binuclear species according to

$$2 >SOH + H_3AsO_4{}^0 = (>SO)_2AsO_2{}^- + H^+ + 2H_2O \quad (10)$$

$${}^*K^\theta_{(>SO)_2AsO_2^-} = \frac{a_{(>SO)_2AsO_2^-} a_{H^+} a^2_{H_2O}}{a^2_{>SOH} a_{H_3AsO_4{}^0}} 10^{\frac{F(\Delta\Psi_{r,10})}{2.303RT}} \quad (11)$$

a protonated bidentate-binuclear species according to

$$2 >SOH + H_3AsO_4{}^0 = (>SO)_2AsOOH + 2H_2O \quad (12)$$

$${}^*K^\theta_{(>SO)_2AsOOH} = \frac{a_{(>SO)_2AsOOH} a^2_{H_2O}}{a^2_{>SOH} a_{H_3AsO_4{}^0}} 10^{\frac{F(\Delta\Psi_{r,12})}{2.303RT}} \quad (13)$$

and a deprotonated monodentate species according to

$$> SOH + H_3AsO_4{}^0 = >SOAsO_3{}^{2-} + 2H^+ + H_2O \quad (14)$$

$${}^*K^\theta_{>SOAsO_3^{2-}} = \frac{a_{>SOAsO_3^{2-}} a^2_{H^+} a_{H_2O}}{a_{>SOH} a_{H_3AsO_4{}^0}} 10^{\frac{F(\Delta\Psi_{r,14})}{2.303RT}} \quad (15)$$

Here, the superscript "$\theta$" again represents site-occupancy standard states (Sverjensky, 2003, 2005). The exponential terms contain the electrostatic factor, $\Delta\Psi_r$, which is a reaction property arising from the work done in an electric field when species in the reaction move on or off the charged surface. It is evaluated taking into account the adsorbing ions and the water dipoles released in Eqs. (10), (12) and (14). Electrostatic work is done in both instances and is reflected in the formulation of $\Delta\Psi_r$ (Sverjensky and Fukushi, 2006a,b).

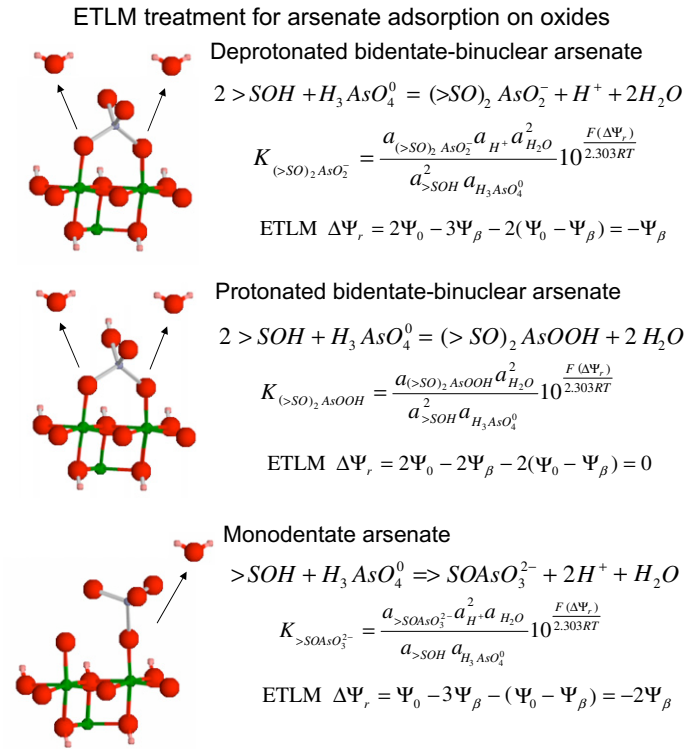


Fig. 1. Diagrammatic representations and model reactions forming arsenate surface species derived from in situ spectroscopic evidence and molecular calculations. The three species form by ligand exchange reactions releasing one or two water dipoles. This effect is taken into account in the electrostatic term for the reaction ($\Delta\psi_r$), which includes contributions from the ions and the specific number of water dipoles released in the reactions.

We place the charge of the adsorbing protons on the 0-plane and the charge of the oxyanion on the β-plane. This is a departure from the practice of placing the oxyanion charge on the 0-plane for inner-sphere complexes in the TLM (Hayes et al., 1988). In our calculations, with the dipole modification and the arsenate or protonated arsenate charge on the β-plane, the ETLM is able to describe a wide variety of arsenate adsorption data. As noted below, the same location for the charge has recently been used for arsenate adsorption on hematite (Arai et al., 2004). For the sake of completeness, we have also included in the present paper some model calculations in which the arsenate or protonated arsenate are placed on the 0-plane (as originally advocated by Hayes et al.) in conjunction with our dipole correction. This approach results in very poor fits to adsorption and surface proton titration data (see below).

In the ETLM, the water dipole(s) leaving the charged surface experience a change in potential equal to $-n(\Psi_0 - \Psi_\beta)$ where $n$ is the number of desorbed waters per reaction. For the reactions in Eqs. (11), (13) and (15), this results in

$$\Delta\Psi_{r,10} = 2\Psi_0 - 3\Psi_\beta - 2(\Psi_0 - \Psi_\beta) = -\Psi_\beta \quad (16)$$

$$\Delta\Psi_{r,12} = 2\Psi_0 - 2\Psi_\beta - 2(\Psi_0 - \Psi_\beta) = 0 \quad (17)$$

$$\Delta\Psi_{r,14} = \Psi_0 - 3\Psi_\beta - (\Psi_0 - \Psi_\beta) = -2\Psi_\beta \quad (18)$$

Interestingly, Eq. (16) is the same overall result for $\Delta\Psi_r$ as found in a recent study using the CD-TLM approach for arsenate on hematite (Arai et al., 2004). In the latter study, it was found by regression of adsorption data that $\Delta\Psi_{10} = -\Psi_\beta$ fitted the data better than alternate fractional distributions of charge. In this study we explain $\Delta\Psi_{r,10} = -\Psi_\beta$ in terms of the dipole correction to the TLM without the need for a CD approach.

We wish to emphasize here that alternate states of arsenate reaction stoichiometry could not fit the bulk arsenate adsorption data. In particular, the mononuclear mono- or diprotonated arsenate surface species did not yield as good a fit to the experimental adsorption and surface titration data. Having said this, it is still true that surface species in addition to those given in Fig. 1 may be present in the real systems, but difficult to detect using surface complexation models. This possibility arises when two different surface species have extremely similar, if not identical, reaction stoichiometries. For example, a bidentate-mononuclear arsenate species (suggested by some X-ray studies, see above) is clearly not included in Fig. 1. However, such a species could have a reaction stoichiometry such as

$$>S(OH)_2 + H_3AsO_4^0 = >SO_2AsO_2^- + H^+ + 2H_2O \quad (19)$$

which is so similar to that in Eq. (10) that it would be difficult to detect the difference in a surface complexation model without examining data referring to a very wide range of surface coverages. Another possible reaction stoichiometry for a bidentate-mononuclear species would be

$$>SOH + H_3AsO_4^0 = >SO_2AsO_2^{2-} + 2H^+ + H_2O \quad (20)$$

which has the same reaction stoichiometry as that in Eq. (14). However, the reaction in Eq. (20) involves a coordination increase for the surface metal, which may be detectable through the comparison of theoretical molecular calculations with infrared data (e.g. Yoon et al., 2004).

Another interesting possibility involves outer-sphere or H-bonded surface species. All the above arsenate surface reactions involve inner-sphere species. Until recently, no outer-sphere-type surface species for arsenate had been directly detected in experimental spectroscopic studies. The recent reports of such a species (Catalano et al., 2006a,b) are of great interest because they bring arsenate surface speciation in line with almost all other oxyanions for which both inner- and outer-sphere (or H-bonded) species have been reported. In our study, we have examined many possible speciation schemes involving different inner- and outer-sphere (or H-bonded) species for consistency with the bulk adsorption data, and have only come up with one possible reaction stoichiometry for an outer-sphere (or H-bonded species) given by

$$2>\mathrm{SOH} + \mathrm{H_3AsO_4}^0 = (>\mathrm{SOH})_2\text{–}\mathrm{AsO_2(OH)_2}^- + \mathrm{H}^+ \tag{21}$$

$${}^*K^{\theta}_{(>\mathrm{SOH})_2\text{–}\mathrm{AsO_2(OH)_2}^-} = \frac{a_{(>\mathrm{SOH})_2\text{–}\mathrm{AsO_2(OH)_2}^-}\, a_{\mathrm{H}^+}}{a^2_{>\mathrm{SOH}}\, a_{\mathrm{H_3AsO_4}^0}}\, 10^{\frac{F(\Delta\Psi_{r,21})}{2.303RT}} \tag{22}$$

$$\Delta\Psi_{r,21} = -\Psi_{\beta} \tag{23}$$

It can be seen that Eq. (21) differs from Eq. (10) only by the release of two waters in the latter reaction. For example, subtracting Eq. (21) from (10) gives

$$(>\mathrm{SOH})_2\text{–}\mathrm{AsO_2(OH)_2}^- = (>\mathrm{SO})_2\mathrm{AsO_2}^- + 2\mathrm{H_2O} \tag{24}$$

$$K^{\theta} = \frac{a_{(>\mathrm{SO})_2\mathrm{AsO_2}^-}}{a_{(>\mathrm{SOH})_2\text{–}\mathrm{AsO_2(OH)_2}^-}}\, a^2_{\mathrm{H_2O}} \tag{25}$$

Based on Eqs. (24) and (25), it can be expected that the relative activities of the two arsenate surface species will be a function of the activity of water only. The ratio should be independent of pH and surface loading. It is interesting to note that preliminary experimental studies indicate that the ratio of the inner- and outer-sphere arsenate surface species is experimentally insensitive to the arsenate concentration in solution (Catalano et al., 2006b), which is consistent with Eqs. (24) and (25). Large variations in ionic strength might affect the activity of water, and hence the relative activities of the arsenate species, but would still be difficult to detect by surface complexation modeling. Overall, we wish to emphasize that it is the relative importance of the three reaction stoichiometries in Fig. 1 that we can establish in our analysis of bulk experimental data. Additional surface species such as those described above may also be present in experimental systems, but would require additional experimental results to establish their relative importance.

The relationships of the site-occupancy standard states to the hypothetical 1.0 M standard state for the arsenic surface species are given by

$$\log {}^*K^{\theta}_{(>\mathrm{SO})_2\mathrm{AsO_2}^-} = \log {}^*K^{0}_{(>\mathrm{SO})_2\mathrm{AsO_2}^-} + \log\left(\frac{(N_S A_S)^2}{N^{\ddagger}A^{\ddagger}} C_S\right) \tag{26}$$

$$\log {}^*K^{\theta}_{(>\mathrm{SO})_2\mathrm{AsOOH}} = \log {}^*K^{0}_{(>\mathrm{SO})_2\mathrm{AsOOH}} + \log\left(\frac{(N_S A_S)^2}{N^{\ddagger}A^{\ddagger}} C_S\right) \tag{27}$$

$$\log {}^*K^{\theta}_{>\mathrm{SOAsO_3}^{2-}} = \log {}^*K^{0}_{>\mathrm{SOAsO_3}^{2-}} + \log\left(\frac{N_S \mathrm{A_S}}{N^{\ddagger}A^{\ddagger}}\right) \tag{28}$$

where $C_S$ denotes solid concentration (g $\mathrm{L}^{-1}$).

The equilibrium constants represented relative to the species >SOH, expressed by the superscript "*" in Eqs. (11), (13) and (15), depend on the $\mathrm{pH_{ZPC}}$ and $\mathrm{p}K^{\theta}_n$ of solid samples. It is convenient to correct for differences in the $\mathrm{pH_{ZPC}}$ and $\mathrm{p}K^{\theta}_n$ with the following equations (Sverjensky, 2005):

$$\log K^{\theta}_{(>\mathrm{SO})_2\mathrm{AsO_2}^-} = \log {}^*K^{\theta}_{(>\mathrm{SO})_2\mathrm{AsO_2}^-} - 2\mathrm{pH_{ZPC}} + \mathrm{p}K^{\theta}_n \tag{29}$$

$$\log K^{\theta}_{(>\mathrm{SO})_2\mathrm{AsOOH}} = \log {}^*K^{\theta}_{(>\mathrm{SO})_2\mathrm{AsOOH}} - 2\mathrm{pH_{ZPC}} + \mathrm{p}K^{\theta}_n \tag{30}$$

$$\log K^{\theta}_{>\mathrm{SOAsO_3}^{2-}} = \log {}^*K^{\theta}_{>\mathrm{SOAsO_3}^{2-}} - \mathrm{pH_{ZPC}} + \frac{\mathrm{p}K^{\theta}_n}{2} \tag{31}$$

The resultant values of $K^{\theta}_{(>\mathrm{SO})_2\mathrm{AsO_2}^-}$, $K^{\theta}_{(>\mathrm{SO})_2\mathrm{AsOOH}}$ and $K^{\theta}_{>\mathrm{SOAsO_3}^{2-}}$ are independent of the site density, surface area or solid concentration of the specific samples, as well as the $\mathrm{pH_{ZPC}}$ and $\mathrm{p}K^{\theta}_n$ used in the experiments. Values of the logarithms of the above equilibrium constants are summarized in Table 2.

### 2.3. Uncertainties in experimental data and regression procedures

The assessment of uncertainties in individual experimental datasets involving arsenate is often not provided by the experimentalists. However, as a guide, the reproducibility of the percent As(V) adsorbed on goethite reported by Gao and Mucci (2001) was about ±3% of the total As. It is likely that at low extents of adsorption the uncertainties would be significantly greater. Unless otherwise stated, these uncertainties have been used as a guide in the analysis discussed below, resulting in an overall uncertainty for the $\log {}^*K^0_j$ values of adsorption of the $j$th arsenate species of about ±0.3. Uncertainties in values of $\log K^{\theta}_j$, calculated with Eqs. (29)–(31) will be significantly larger because of uncertainties in the values of $\mathrm{p}K^{\theta}_n$ and $\mathrm{pH_{ZPC}}$ and may be of the order of ±0.5. In some cases, where experimental data for adsorption over a range of surface coverages as well as a range of pH and ionic strength values were available, equilibrium constants and site densities were derived simultaneously. The uncertainties in the resultant equilibrium constants are within those cited above (see also in the discussion given below).

Regression of a wide variety of experimental data including adsorption envelope, isotherm, proton surface titration and proton coadsorption of arsenate discussed below was carried out by direct simulation of the experimental data generating values of the equilibrium constants $\log {}^*K^0_j$ (and, in some instances site densities). In the absence of quantitative measures of uncertainty in the experimental studies, each dataset was regressed taking into account the general uncer-

Table 2
Equilibrium constants for As(V) adsorption from regression of the data in Figs. 2–5 and 7–12

| Solid | $\varepsilon_s$ [a] | $N_s$ nm$^{-1}$ | log $^*K^0_{>SOAsO_4^{2-}}$ | log $K^\theta_{>SOAsO_4^{3-}}$ | $C_s$ g L$^{-1}$ | log $^*K^0_{(>SO)_2AsO_2^-}$ | log $K^\theta_{(>SO)_2AsO_2^-}$ | log $^*K^0_{(>SO)_2AsOOH}$ | log $K^\theta_{(>SO)_2AsOOH}$ | Adsorption data | Data |
|---|---|---|---|---|---|---|---|---|---|---|---|
| HFO | 1000 | 3.8 | 3.9 | 0.2 | 0.03 | 12.0 | 5.0 | 13.5 | 6.5 | Dixit and Hering (2003) | Fig. 7 |
| Ferrihydrite | 32 | 3.8 | 3.5 | −0.8 | 2 | 10.4 | 4.0 | 12.0 | 5.6 | Jain et al. (1999, 2000) | Fig. 8[b] |
| FeOOH | 15 | 3.5 | 2.5 | −3.6 | 0.5 | 11.0 | 0.5 | 13.7 | 3.2 | Dixit and Hering (2003) | Fig. 2[c] |
| FeOOH | 15 | 4.5 | 2.0 | −3.6 | 0.234 | 12.6 | 2.8 | 13.9 | 4.1 | Gao and Mucci (2001) | Fig. 3 |
| FeOOH | 15 | 3.5 | 6.0 | −0.1 | 1 | 12.2 | 2.0 | 13.0 | 2.8 | Antelo et al. (2005) | Fig. 4 |
| FeOOH | 15 | 3.5 | 6.0 | −0.1 | 0.333 | 12.7 | 2.0 | 13.5 | 2.8 | Antelo et al. (2005) | Fig. 4 |
| FeOOH | 15 | 3.9 | 2.0 | −3.7 | 2.5 | 8.5 | −0.4 | 10.9 | 2.0 | Manning and Goldberg (1996) | Fig. 5 |
| α-$Al_2O_3$ | 10.4 | 3.0 | −1.8 | −8.7 | 10 | 8.4 | −2.4 | 10.0 | −0.8 | Halter and Pfeifer (2001) | Fig. 12 |
| β-$Al(OH)_3$ | 10.3 | 5.0 | −2.0 | −7.8 | 5 | 7.2 | −1.8 | 7.0 | −2.0 | Arai et al. (2001) | Fig. 10 |
| am·AlO | 10.3 | 2.5 | −1.5 | −6.9 | 4 | 8.4 | 0.2 | 11.6 | 3.4 | Goldberg and Johnston (2001) | Fig. 9 |
| am·AlO | 10.3 | 2.5 | −1.5 | −6.9 | 0.5 | 9.3 | 0.2 | 12.5 | 3.4 | Goldberg and Johnston (2001) | Fig. 9 |
| α-$Al(OH)_3$ | 8.4 | 3.0 | −2.0 | −8.9 | 2.5 | 9.0 | −2.3 | 9.5 | −1.8 | Manning and Goldberg (1996) | Fig. 11 |

Values of log $^*K^0_{>SOAsO_3^{2-}}$, log $^*K^0_{(>SO)_2AsO_2^-}$ and log $^*K^0_{(>SO)_2AsOOH}$ refer to the hypothetical 1.0 M standard state and reactions formed from >SOH ($\log {}^*K^0_{>SOAsO_3^{2-}}$ : $> SOH + H_3AsO_4 = > SOAsO_3^{2-} + 2H^+ + H_2O$; $\log {}^*K^0_{(>SO)_2AsO_2^-}$ : $2 > SOH + H_3AsO_4 = (> SO)_2AsO_2^- + H^+ + 2H_2O$; $\log {}^*K^0_{(>SO)_2AsOOH}$ : $2 > SOH + H_3AsO_4 = (> SO)_2AsOOH + 2H_2O$). Values of log $K^\theta_{>SOAsO_3^{2-}}$, log $K^\theta_{(>SO)_2AsO_2^-}$ and log $K^\theta_{(>SO)_2AsOOH}$ refer to site-occupancy standard states for As(V) adsorption reactions ($\log K^\theta_{>SOAsO_3^{2-}}$ : $> SOH_2^+ + H_3AsO_4 = > SOAsO_3^{2-} + 3H^+ + H_2O$; $\log K^\theta_{(>SO)_2AsO_2^-}$ : $2 > SOH_2^+ + H_3AsO_4 = (> SO)_2AsO_2^- + 3H^+ + 2H_2O$; $K \log K^\theta_{(>SO)_2AsOOH}$ : $2 > SOH_2^+ + H_3AsO_4 = (> SO)_2AsOOH + 2H^+ + 2H_2O$) calculated from the values of log $^*K^0_{>SOAsO_3^{2-}}$, log $^*K^0_{(>SO)_2AsO_2^-}$ and log $^*K^0_{(>SO)_2AsOOH}$ with aid of Eqs. (26)–(28) and (29)–(31) using values of $N_S$, $A_S$, $pH_{ZPC}$ and $\Delta pK^\theta_n$ from Table 1 and $C_S$ from Table 2.

[a] Solid dielectric constant after Sverjensky and Fukushi (2006b).

[b] The dashed curves is computed with $\Delta\psi_r = -3\psi_0 + \psi_\beta$ for $>SOAsO_3^{3-}$, $\Delta\psi_r = -3\psi_0 + 2\psi_\beta$ for $(>SO)_2\ AsO_2^-$ and $\Delta\psi_r = -2\psi_0 - 2\psi_\beta$ for $(>SO)_2AsOOH$. Values for log $^*K^0_{>SOAsO_3^{2-}}$, log $^*K^0_{(>SO)_2AsO_2^-}$ and log $^*K^0_{(>SO)_2AsOOH}$ are 4.5, 10.0 and 25.0, respectively.

[c] The dashed curves were computed with $\Delta\psi_r = -3\psi_0 + \psi_\beta$ for $>SOAsO_3^{2-}$, $\Delta\psi_r = -3\psi_0 + 2\psi_\beta$ for $(>SO)_2\ AsO_2^-$ and $\Delta\psi_r = -2\psi_0 + 2\psi_\beta$ for $(>SO)_2\ AsOOH$. Values for log $^*K^0_{>SOAsO_3^{2-}}$, log $^*K^0_{(>SO)_2AsO_2^-}$ and log $^*K^0_{(>SO)_2AsOOH}$ are 1.5, 10.0 and 10.0, respectively.

tainties indicated above, as well as apparent scatter in the experimental results. An iterative regression approach was used to ensure the consistency of regression results for different types of experimental data in a given system. Conversion of the values of log ${}^{*}K_j^0$ to values of log $K_j^\theta$ (referring to site-occupancy standard states) enabled direct comparison of the results of experimental studies of different samples of the same type of solid as well as arsenate adsorption on different solids. These differences are analysed below. In this way the experimental results for arsenate adsorption in many different laboratories can be integrated into a single predictive description.

## 3. APPLICATION TO ARSENATE ADSORPTION

### 3.1. Adsorption of arsenate on goethite from Dixit and Hering (2003), Gao and Mucci (2003), Antelo et al. (2005), Manning and Goldberg (1996)

Arsenate adsorption data are analyzed below for four synthetic goethites (Table 1) chosen because they refer to a wide range of arsenate adsorption conditions. Of these, only one (Antelo et al., 2005) excluded $CO_2$ during the synthesis of the goethite and during the arsenate adsorption study. However, the Dixit and Hering (2003) study tried several experiments with and without $CO_2$ present and found no significant difference in arsenate adsorption. Similarly, Arai et al. (2004) demonstrated that only partial pressures of carbon dioxide higher than atmospheric affected arsenate adsorption significantly. Data for a fifth goethite (Rietra et al., 1999), referring to a narrow range of conditions of arsenate and proton coadsorption are considered below as a test of the predictive correlations to be discussed below.

The adsorption data depicted in Fig. 2a and b refer to arsenate adsorption envelopes over a range of surface coverages and an adsorption isotherm on goethite at a single ionic strength (Dixit and Hering, 2003). The solid curves in Fig. 2a and b represent regression calculations using the three reactions given in Fig. 1. It should be emphasized that the site density used in the present calculations was not a regression parameter. Only the three equilibrium constants were regression parameters. The site density was taken from independent ETLM analysis of arsenite adsorption on the same goethite (Sverjensky and Fukushi, 2006a,b). It can be seen in Fig. 2a that the solid curves provide a close description of the arsenate adsorption data over a wide range of pH and surface coverage (error bars are not reported in the study by Dixit and Hering, 2003).

The solid points in Fig. 2b represent the two highest surface coverages at pH 4 in Fig. 2a (50 and 100 μM of arsenate). The two lowest coverage data are not included in Fig. 2b because of high uncertainties of the aqueous arsenate concentrations near 100% adsorption. It can be seen in Fig. 2b that although the model calculation provides a close description of much of the isotherm data, it systematically underestimates the amount of adsorbed arsenate at surface coverages above approximately $10^{-5.6}$ mol.m$^{-2}$ (2.5 μmol m$^{-2}$). Under these conditions, arsenate apparently accumulates at the surface through processes other than adsorption alone, for example surface precipitation, surface polymerization or diffusion into the structure (Raven et al., 1998; Jain et al., 1999; Stanforth, 1999; Zhang and Stanforth, 2005; Jia et al., 2006).

The predicted surface speciation as a function of pH and surface coverage at the highest and lowest arsenate concentrations in Fig. 2a can be seen in Fig. 2c and d. These predictions serve as a test of the model which can be compared with qualitative trends in speciation with pH and surface coverage defined spectroscopically which were not used in the regression calculations. In Fig. 2c, which refers to a relatively high surface coverage (2.2 μmol m$^{-2}$ at 60% adsorption), the protonated bidentate-binuclear species is predicted to predominate at the lowest pH values of 3–5, and the deprotonated bidentate-binuclear species at pH values of 5–8. This agrees remarkably well with trends inferred from the *in situ* FTIR study of phosphate on goethite at similar surface coverages (1.9–2.3 μmol m$^{-2}$, (Tejedor-Tejedor and Anderson, 1990): a protonated bidentate-binuclear species at pH 3.6 to 5.5–6.0 and a deprotonated bidentate-binuclear species between pH values of about 6–8.3.

It can also be seen in Fig. 2c that the relative importance of the mononuclear species increases with pH and it predominates at pH values of 9–10. At the lower surface coverage of Fig. 2d, 0.37 μmol m$^{-2}$ at 100% adsorption, it can be seen that the mononuclear species is predicted to dominate from pH values of about 4.5–10. Both trends are consistent with inferences about the relative importance of the mononuclear species from EXAFS and IR spectroscopy as a function of oxyanion loading and pH (Tejedor-Tejedor and Anderson, 1990; Waychunas et al., 1993; Fendorf et al., 1997). It should be noted that the mononuclear species was not detected in other EXAFS studies (Farquhar et al., 2002; Sherman and Randall, 2003). However, Farquhar et al. (2002) obtained their spectra for adsorption conditions of pH 5.5–6.5 and coverage of 6 μmol m$^{-2}$, and Sherman and Randall (2003) used adsorption conditions of pH 3.9 and 1 μmol m$^{-2}$. Under these conditions, the present calculations indicate that the mononuclear species should not be important compared to the bidentate-binuclear species.

Overall, the predictions depicted in Figs. 2c and d agree very well with the speciation trends indicated by the independently established *in situ* FTIR and X-ray studies of phosphate and arsenate on goethite, which provides strong support for the model reactions proposed in Fig. 1. It also indicates that the surface chemistry of the Dixit and Hering (2003) goethite (with respect to arsenate speciation) is consistent with the surface chemistry of the goethites synthesized by Farquhar et al. (2002), Fendorf et al. (1997), Sherman and Randall (2003), Tejedor-Tejedor and Anderson (1990) and Waychunas et al. (1993). Similar predicted trends of surface speciation were found using the CD model approach for phosphate surface complexation on goethite (Hiemstra and van Riemsdijk, 1999). It will be shown below that experimental results for arsenate on another very similar goethite from the van Riemsdijk laboratory (in Rietra et al., 1999) are also consistent with the type of speciation discussed above and typified by the model results for the Dixit and Hering (2003) goethite.

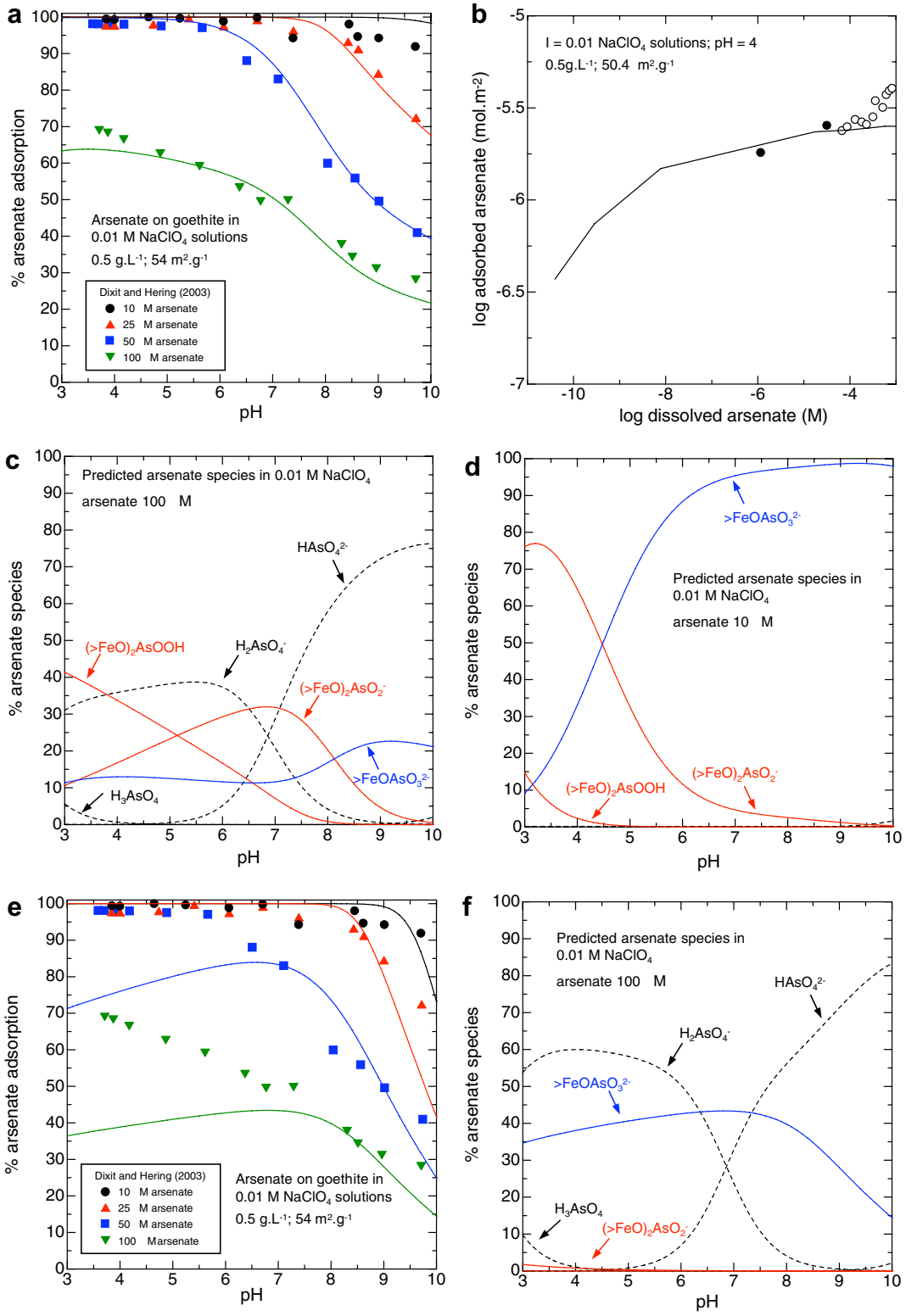


Fig. 2. The data points represent experimental results for arsenate adsorption on goethite from Dixit and Hering (2003). The curves in (a) and (b) represent regression calculations, but those in (c) and (d) represent predictions made with the ETLM using the arsenate surface species and parameters in Tables 1 and 2. (a) Arsenate adsorption as a function of pH and surface coverage. (b) Arsenate adsorption as a function of arsenate loading. (c,d) Predicted model arsenate surface and aqueous speciation. The proportion of monodentate species increases with pH, but decreases with surface coverage consistent with *in situ* X-ray and infrared results. (e,f) Regression of adsorption data and predicted surface speciation obtained with an alternate approach in which the arsenate charge is placed on the 0-plane and the water dipole correction is applied as in the ETLM. Parameters used are given in Table 2 footnotes.

The data in Fig. 2a also permit a test of an alternate approach to the surface complexation modeling described above. If instead of placing the charge of the arsenate or biarsenate ion on the β-plane, it is placed on the 0-plane, in conjunction with the same water dipole correction described above, the values of $\Delta\Psi_r$ in Eqs. (11), (13) and (15) become equal to $-3\Psi_0 - 2\Psi_\beta$, $-2\Psi_0 - 2\Psi_\beta$, and $-3\Psi_0 + \Psi_\beta$, respectively (Footnote in Table 2). The results of applying this approach to the adsorption data are depicted in Fig. 2e. The calculated model curves in Fig. 2e do not have the correct shape to fit the data adequately (another example of the poor model behavior associated with the 0-plane assumption is given below). The predicted surface speciation for the highest surface coverage in Fig. 2e is shown in Fig. 2f. It can be seen that the predominant species is the mononuclear species, in contrast to the corresponding ETLM calculation shown in Fig. 2c.

Fig. 3a and b show experimental proton surface titration and arsenate adsorption data on goethite at much higher ionic strengths (Gao and Mucci, 2001). The solid curves in Fig. 3b represent regression calculations with the ETLM again using the surface species from Fig. 1. In these calculations, the site density was retrieved together with the three equilibrium constants for arsenate adsorption. Predicted surface speciation plots are shown in Fig. 3c and d for the highest and lowest surface coverages from Fig. 3b. It can be seen that the deprotonated bidentate species is dominant except at the highest and lowest pH conditions. As in Fig. 2c and d, the protonated bidentate-binuclear species becomes important at low pH conditions whereas the importance of the monodentate species increases with pH and decreases with surface coverage. However, in contrast to the goethite in Fig. 2c and d, the mononuclear species in Fig. 3c and d is dominant only at pH values above 9. A direct comparison between the Dixit and Hering goethite and the Gao and Mucci goethite can be made using Figs. 2d and 3e, which are constructed for the same ionic strength and surface coverage. It can clearly be seen that the predicted surface speciations for the two goethites differ significantly (see below).

Experimental surface titration and arsenate adsorption isotherm data for a third goethite from Antelo et al. (2005) are depicted in Fig. 4a–c. Experimental uncertainties are not cited by the authors for these data, nevertheless it can be seen in Fig. 4b and c that the solid regression curves generated in the present study provide a representation of the data within about 10%. In these calculations, the site density and the equilibrium constants for arsenate adsorption were all obtained. The predicted speciation plots in Fig. 4d–f show a marked predominance of the monodenate-mononuclear species at high pH values. In particular, Fig. 4f was constructed to represent the same conditions as in Figs. 2d and 3e in order to directly compare the three goethites. It can be seen in Fig. 4f that the Antelo et al. goethite shows an extremely high predominance of the mononuclear species. In this regard, it forms an end-member for the goethites analyzed in the present study. It is interesting to note recent preliminary ATR-FTIR spectroscopic reports of mononuclear phosphate and arsenate on goethite (Loring et al., 2006; Nelson et al., 2006). On hematite, *in situ* ATR-FTIR results have also been interpreted in terms of possible mononuclear protonated and deprotonated phosphate complexes, although at least one of these was suggested to have been "bridging" in the sense of being strongly H-bonded to a second Fe-octahedron (Elzinga and Sparks, 2007).

Experimental arsenate adsorption data for a fourth goethite (Manning and Goldberg, 1996) are depicted in Fig. 5a. The solid curves in Fig. 5a again represent regression calculations using the reactions in Fig. 1. In these calculations, a predicted site density was used based on the linear correlation between site density and BET surface area for goethites developed previously (Fukushi and Sverjensky, 2007). It can be seen in Fig. 5a that the calculated curve for the higher arsenate concentration results in a significant underestimation of the amount adsorbed at pH values less than 4.5, which may indicate the need for an additional surface species of arsenate. In contrast, the calculated curve for the lower arsenate concentration slightly overestimates the amount adsorbed at pH values above 9.

Predicted speciation plots for the goethite studied by Manning and Goldberg (1996) are shown in Fig. 5b–d. It can be seen in Fig. 5b and c that the surface speciation for this goethite is similar to that shown above for the Dixit and Hering goethite. A more accurate comparison can be made with the aid of Fig. 5d, where the surface coverage and ionic strength are the same as in Fig. 2d. The speciation in Fig. 5d is actually intermediate between the speciation for that shown in Fig. 2d and the Antelo et al. goethite in Fig. 4f.

In summary, our model speciation results for the behavior of arsenate adsorption on the four goethites studied here vary quite markedly. We select the goethite from Dixit and Hering (2003) as a model goethite because the calculated trends in speciation with pH and surface coverage for this goethite agree well with the trends inferred from the infrared and X-ray studies by Farquhar et al. (2002), Fendorf et al. (1997), Sherman and Randall (2003), Tejedor-Tejedor and Anderson (1990), and Waychunas et al. (1993). On our model goethite, binuclear or mononuclear arsenate surface species occur depending on the environmental conditions. In contrast, on the Antelo et al. (2005), Gao and Mucci (2001) and Manning and Goldberg (1996) goethites, the model arsenate surface speciation is dominated either by the binuclear or by the mononuclear surface species, when a consistent set of environmental conditions are compared.

One possible explanation for variation in goethite/arsenate surface chemistry could result from different adsorption characteristics on different crystal faces that may be developed on the different goethite samples. Unfortunately, the proportions of different crystal faces on the samples discussed above are not known. However, comparisons of the different goethites studied here can be made in terms of the site densities derived for arsenate adsorption. It can be seen in Fig. 6 that the site densities of the Antelo et al. (2005), Dixit and Hering (2003) and Gao and Mucci (2001) goethites derived by regression, lie close to the correlation with surface area depicted by the solid line. Estimated uncertainties in the site densities are about $\pm 0.3$ sites nm$^{-2}$. Sensitivity analysis of the regression calculations indicated that such an uncertainty corresponds to about $\pm 0.2$ in the equilibrium constants generated simultaneously. All three are

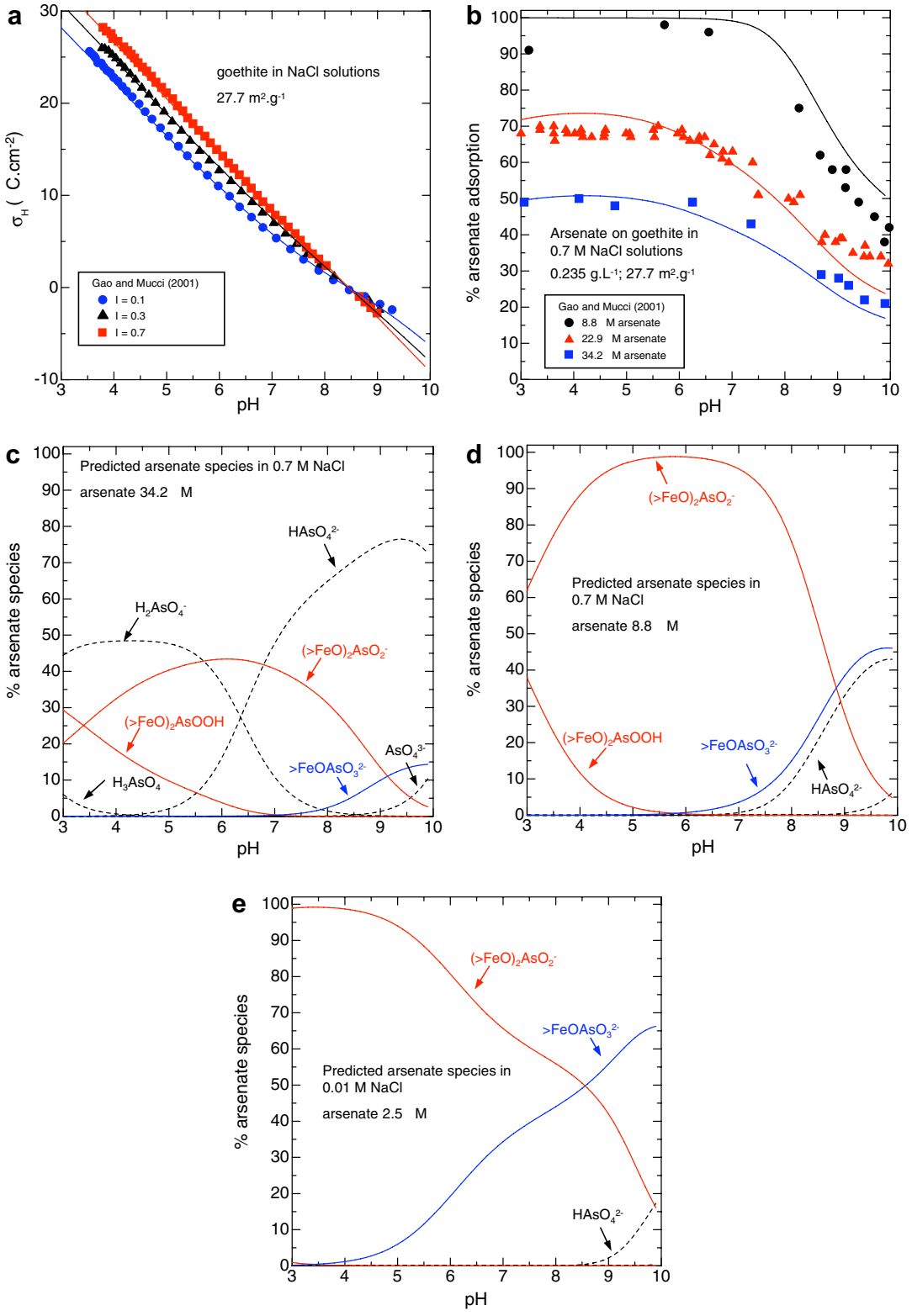


Fig. 3. The data points represent experimental results for proton surface titration and arsenate adsorption on goethite from Gao and Mucci (2001). The solid curves in (a) and (b) represent regression calculations with the ETLM using the arsenate surface species and parameters in Table 1 and 2. (a) Proton surface charge as a function of pH and ionic strength in NaCl solutions. (b) Arsenate adsorption as a function of pH and surface coverage. (c,d) Predicted model arsenate surface and aqueous speciation. (e) Predicted arsenate speciation for the same conditions as in Fig. 2d. Note the increased predominance of the bidentate-binuclear arsenate species.

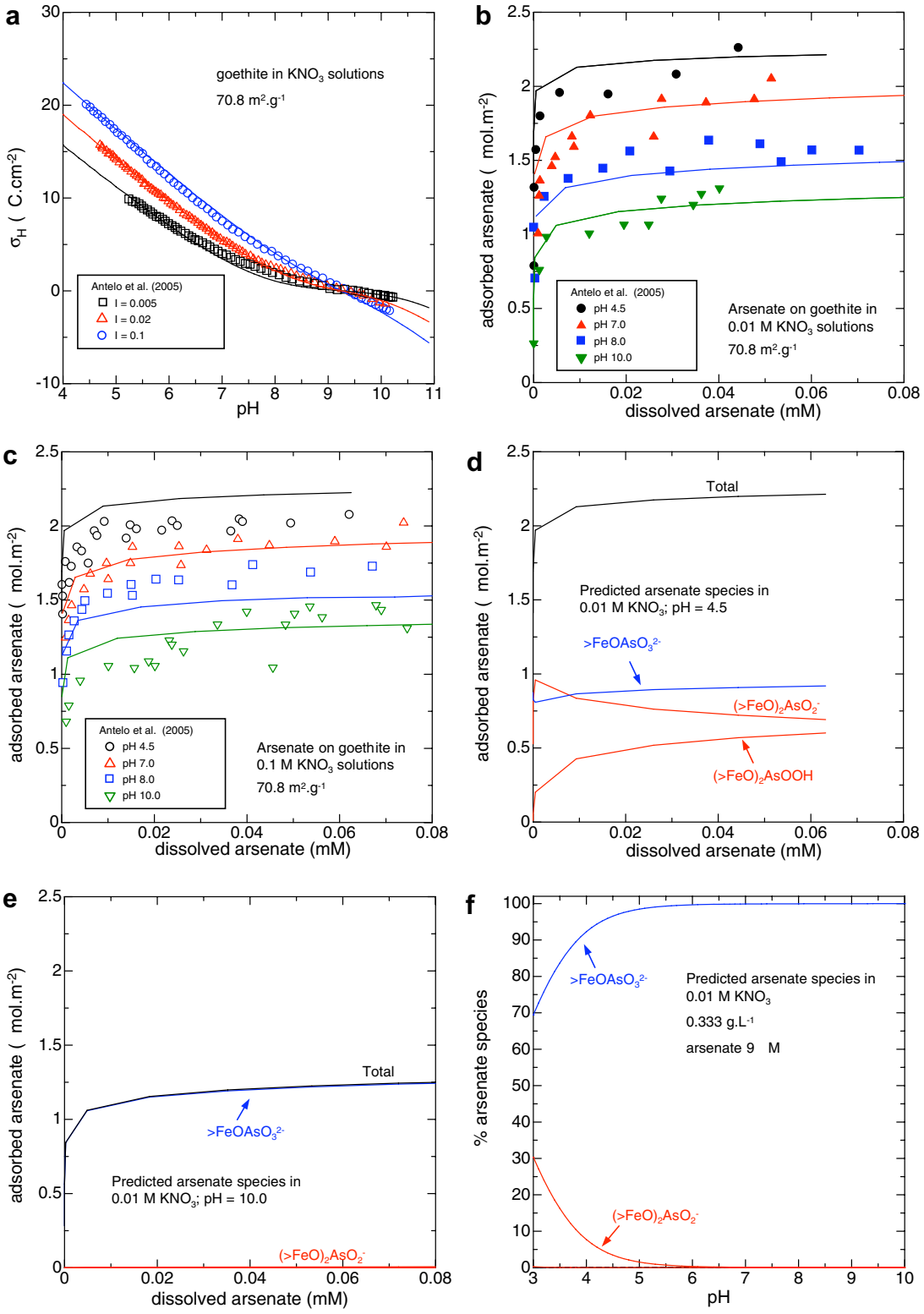


Fig. 4. The data represent experimental results for arsenate adsorption on goethite from Antelo et al. (2005). The curves in (a)–(c) represent regression calculations but those in (d)–(f) represent predictions made with the ETLM using the arsenate surface species and parameters in Table 1 and 2. (a) Proton surface charge as a function of pH and ionic strength without arsenic. (b,c) Arsenate adsorption as a function of arsenate loading at two different ionic strengths. (d,e) Predicted model arsenate surface and aqueous speciation as a function of arsenate loading. (f) Predicted arsenate speciation for the same conditions as in Figs. 2d and 3e. Note the overwhelming predominance of the mononuclear arsenate species compared to that in Fig. 2d.

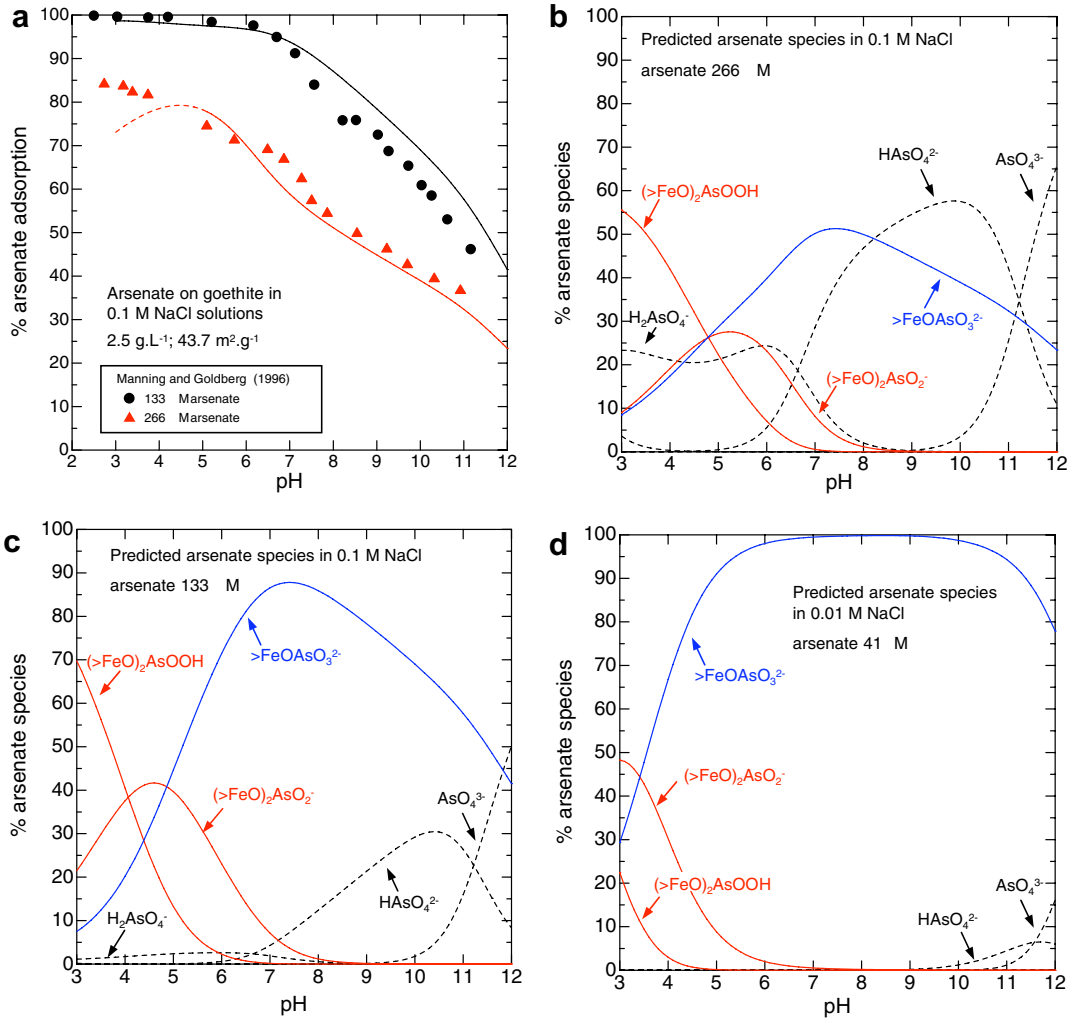


Fig. 5. The data points represent experimental results for arsenate adsorption on goethite from Manning and Goldberg (1996). The solid curves in (a) represent regression calculations with the ETLM using the arsenate surface species and parameters in Table 1 and 2. (a) Arsenate adsorption as a function of pH and surface coverage. (b,c) Predicted model arsenate surface and aqueous speciation. (d) The predicted arsenate speciation referring to the same conditions as in Figs. 2d, 3e and 4f. Note that the speciation here is similar to that in Fig. 2d for the Dixit and Hering goethite but the mononuclear species is more dominant over most of the pH range.

therefore in reasonable agreement with the additional data shown on the plot derived from regression of sulfate and oxalate adsorption data. The negative slope of the line in Fig. 6 is qualitatively consistent with results for carbonate on goethites with different surface areas (Villalobos et al., 2003).

The differences of site densities for the goethites may result from fundamental differences in sample characteristics for each goethite. For example, if arsenate only adsorbs on singly coordinated oxygen groups, e.g. $>O_4FeO(H)$ or $>O_5FeO(H)$ groups (Catalano et al., 2006a,b,c,d, 2007), the availability of these groups will depend on the proportions of different faces making up the surface area of the goethite samples. As already noted, the proportions of different crystal faces for the goethite samples in Fig. 6 are not known, although it has been suggested by Rietra et al. (2001) that their goethite synthesis method produces (1 0 1) and (2 1 0) faces (Pnma space group).

In an independent study of the surface protonation characteristics of goethite, significant differences in the proportions of crystal faces have been demonstrated for two goethites with different surface areas (Gaboriaud and Ehrhardt, 2003). On a goethite with intermediate surface area ($49\ m^2\ g^{-1}$), the (0 0 1) face was much more abundant than the (1 0 1) face (Pnma space group). On a high surface area goethite ($95\ m^2\ g^{-1}$), the reverse distribution was found. The (0 0 1) face of goethite has a site density for singly-coordinated oxygens of 3.3 sites $nm^{-2}$ (Koretsky et al., 1998). However, if we assume that the (0 0 1) face is faceted with (2 1 0) faces (Weidler et al., 1996), which have a site density of 7.4 sites $nm^{-2}$, then the overall site density for the faceted (0 0 1) surface may approach 6–7 sites $nm^{-2}$, depending on the degree of faceting. In contrast, the (1 0 1) face has a much lower site density of singly-coordinated oxygens, 3.0 sites $nm^{-2}$. As a consequence, a goethite with a high proportion of faceted (0 0 1) surfaces relative to (1 0 1) surfaces

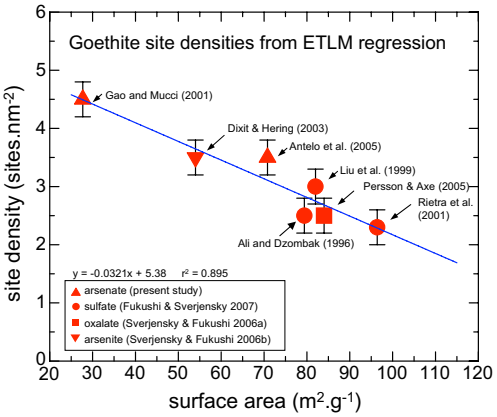


Fig. 6. Empirical correlation of goethite site densities generated with the ETLM by regression of adsorption data referring to a wide range of surface coverages for several different oxyanions (present study; Sverjensky and Fukushi, 2006a,b; Fukushi and Sverjensky, 2007). Sources of the original adsorption data used to generate the site densities are labelled on the figure. Site densities generated in the present study are represented by the solid upright triangles. The negative slope of the line is consistent with likely abundances of singly-coordinated oxygens on different crystal planes (see text). It is also consistent with results obtained for carbonate on goethites with different surface areas by Villalobos et al. (2003).

should have a relatively high site density of singly-coordinated oxygens, i.e. the 49 $m^2\ g^{-1}$ sample referred to above should have a higher oxyanion-determined site density than the 95 $m^2\ g^{-1}$ sample. Qualitatively, this is consistent with and could explain the negative slope of the line in Fig. 6. Lower surface area goethites studied by Prélot et al. (2003) with BET values of 18 and 38 $m^2\ g^{-1}$ also had the (0 0 1) face predominating over the (1 0 1) face, with a terminal (121) face developed. Further work in characterizing all the faces on goethite samples with different surface areas is clearly needed for the actual samples used in adsorption studies.

Another possible explanation for the variation in goethite surface speciation obtained above is contamination by other ferric oxides (e.g. hydrous ferric oxide, HFO). It will be shown below that the model surface speciation for arsenate on HFO and the equilibrium constants of adsorption are significantly different to those of the model goethite of Dixit and Hering discussed above. Our previous ETLM analyses for sulfate and selenate adsorption on goethite also showed significant differences in both site density and $\log K^{\theta}$ values for different goethites (Fukushi and Sverjensky, 2007). Some of these differences were attributed to contamination by atmospheric carbonate (which binds more strongly than sulfate, the opposite to arsenate as noted above) and/or contamination by amorphous hydrous ferric oxides during the synthesis of the specimen, which could change the fundamental surface characteristics of the goethites.

### 3.2. Adsorption of arsenate on HFO from Dixit and Hering (2003)

The adsorption data depicted in Fig. 7a and b refer to arsenate adsorption edges and an isotherm on HFO, respectively (Dixit and Hering, 2003). The solid curves in Fig. 7a and b represent regression calculations using the three reactions in Fig. 1 and a site density used previously for arsenite on the same HFO sample (Sverjensky and Fukushi, 2006b). It can be seen that the calculated curves provide a close description of the arsenate adsorption data over a range of pH and surface coverage except at the conditions of the lowest pH and highest surface coverages (Fig. 7a and b). At pH 4 and surface coverages greater than 2.8 μmol $m^{-2}$ the calculated curves underestimate the amount of arsenic at the surface. This could indicate the need for an additional surface species. However, the isotherm result is very similar to the goethite case discussed above, which was attributed to surface precipitation, polymerization or diffusion in the bulk structure. Jia et al. (2006) have documented surface precipitation of arsenate on ferrihydrite by means of X-ray diffraction and infrared spectroscopy. They showed that surface precipitation of ferric arsenate occurred at pH values of 3–5 and surface coverages of 2.4–9.3 μmol $m^{-2}$, which is in excellent agreement with our estimate of the limit of adsorption based on the ETLM calculations in Fig. 7a and b.

The predicted model speciation of arsenate on HFO surfaces is given in Fig. 7c and d for the highest and lowest surface coverages of Fig. 7a, respectively. For both surface coverages, it can be seen that the bidentate-binuclear species dominate at pH values less than about 8–9. Comparing Fig. 7c with d, it can be seen that the importance of the mononuclear species increases with decreasing surface coverage, which is consistent with the trend indicated by EXAFS spectroscopy of arsenate adsorption on poorly crystalline iron oxide (Waychunas et al., 1993). The protonated bidentate-binuclear species becomes important at low pH values, consistent with IR spectroscopy of phosphate adsorption on ferrihydrite (Arai and Sparks, 2001).

### 3.3. Adsorption of arsenate on ferrihydrite from Jain et al. (1999) and Jain and Loeppert (2000)

A much greater variety of experimental data types are depicted in Fig. 8a–c. These include proton surface charge in the absence and presence of arsenic (Fig. 8a), proton coadsorption with arsenic at two fixed pH values (Fig. 8b), and percent arsenic adsorption (Fig. 8c). The proton surface charge data in the presence of arsenic (Fig. 8a) were obtained from a combination of the titration difference data and the proton surface charge data without arsenic presented in Figs. 2 and 5 of Jain et al. (1999). Adsorption envelope data reported by the same research group (Raven et al., 1998) at lower and higher As loadings than those depicted in Fig. 8c were not used because the lowest surface loadings all result in essentially 100% adsorption and the highest surface loading will be dominated by processes other than adsorption (see below).

Although the uniqueness of surface species for surface complexation modeling has been questioned when only macroscopic percent adsorption data are modeled (Hering and Dixit, 2005), the great variety of types of data in Fig. 8a–c provide strong constraints on the reaction stoichiometries of the arsenate surface species. The solid curves in Fig. 8a–c represent regression calculations again using the

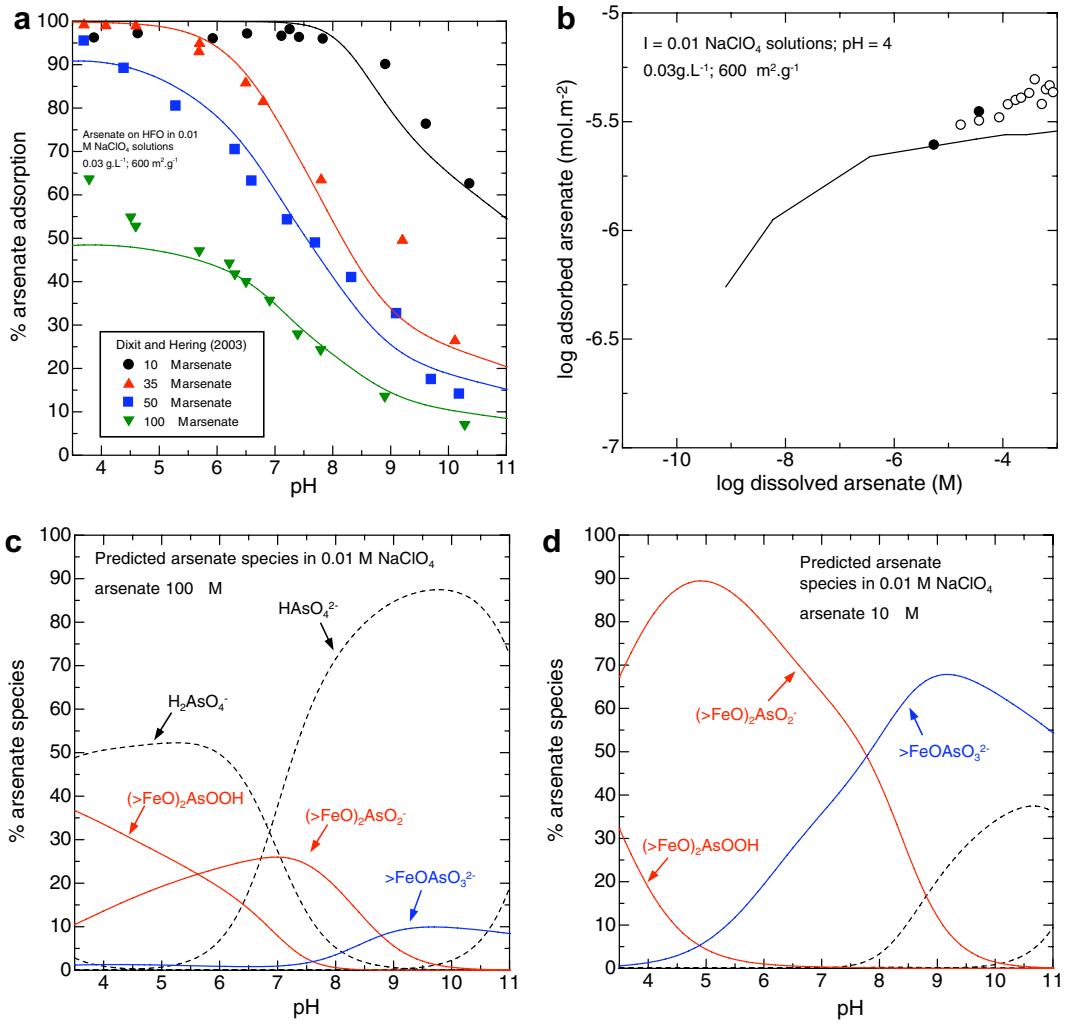


Fig. 7. The data represent experimental results for arsenate adsorption on hydrous ferric oxide (HFO) from Dixit and Hering (2003). The curves in (a) and (b) represent regression calculations but those in (c) and (d) represent predictions made with the ETLM using the arsenate surface species and parameters in Tables 1 and 2. (a) Arsenate adsorption as a function of pH and surface coverage. (b) Arsenate adsorption as a function of arsenate loading. (c,d) Predicted model arsenate surface and aqueous speciation. The proportion of monodentate species increases with pH, but decreases with surface coverage consistent with *in situ* X-ray results (Waychunas et al., 1993).

three reactions in Fig. 1 and the site density used previously for arsenite calculations for this sample (Table 1). Only data represented by the solid symbols were regressed in Fig. 8b and c. Data at higher surface coverages presumably represent processes in addition to adsorption such as surface polymerization or precipitation (Raven et al., 1998; Jain et al., 1999; Jain and Loeppert, 2000; Zhang and Stanforth, 2005; Jia et al., 2006, 2007). For example, in Fig. 8c, the adsorption data at the two highest As(V) loadings represented by the open symbols are systematically underestimated by the dashed calculated curves at pH values less than about 6. Similarly, it can be seen in Fig. 8b that extrapolation of the calculated proton coadsorption curve for pH 4.6 will underestimate the data at surface coverages above about 2.3 μmol $m^{-2}$. It is under acidic conditions that surface precipitation of ferric arsenate has been documented (Jia et al., 2006, 2007). Under other conditions, it can be seen that the solid curves represent a reasonable fit to the data in Fig. 8a–c.

The dashed curves in Fig. 8a represent the alternative approach of placing the arsenate on the 0-plane, as described above for Fig. 2e (see the footnotes to Table 3). This approach is clearly inconsistent with the trends represented by the data.

The predicted surface speciation of arsenate on the surface of ferrihydrite is given in Fig. 8d for one surface coverage from Fig. 8c. It is predicted that the deprotonated bidentate-binuclear species is dominant for most pH conditions. However, the importance of the mononuclear species is again predicted to increase with pH similar to HFO, consistent with EXAFS and IR spectroscopic results (Waychunas et al., 1993; Arai et al., 2001).

### 3.4. Adsorption of arsenate on amorphous aluminum oxide (am·AlO) from Goldberg and Johnston (2001)

The data depicted in Fig. 9a show arsenate adsorption envelopes on am·AlO as functions of pH, ionic strength

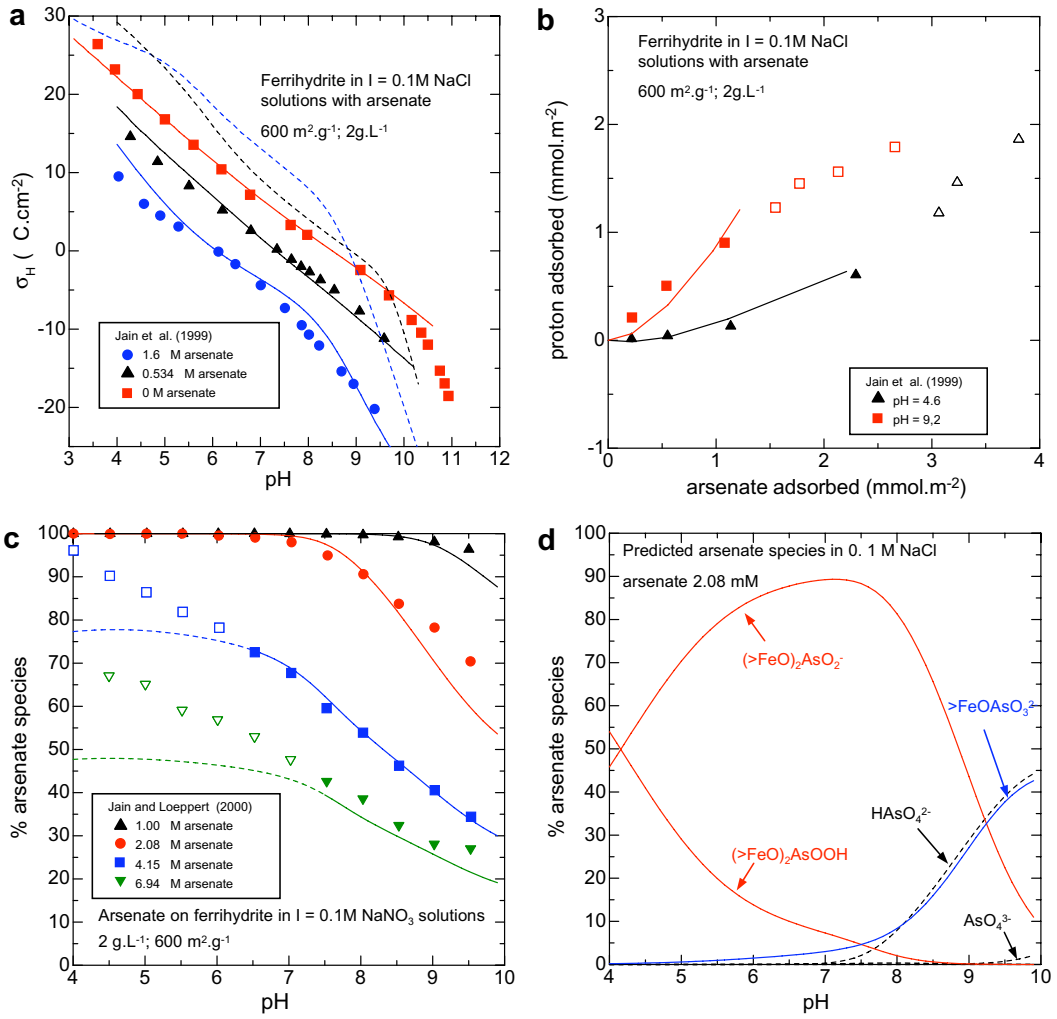


Fig. 8. The data points represent experimental results for arsenate adsorption on ferrihydrite from Jain et al. (1999) and Jain and Loeppert (2000). The solid curves in (a)–(c). represent regression calculations with the ETLM using the arsenate surface species and parameters in Table 1 and 2. Only the data represented by the solid symbols were regressed. The data represented by the open symbols likely represent sorption processes additional to adsorption. The dashed curves in (a) were obtained by regression with an alternate approach in which the arsenate charge is placed on the 0-plane and the water dipole correction is used as in the ETLM (the parameters used are given in Table 2 footnotes). (a) Proton surface charge as a function of pH with and without arsenate. (b) Proton coadsorption with arsenate. (c) Arsenate adsorption as a function of pH and surface coverage. (d) Predicted model arsenate surface and aqueous speciation.

and surface coverage. The solid curves in Fig. 9a represent regression calculations using the three reactions in Fig. 1 and the same site density used previously for arsenite calculations for this sample (Table 1). The calculated curves provide a close description of the arsenate adsorption data. In addition to the adsorption data, Goldberg and Johnston (2001) measured electrophoretic mobilities of am·AlO with and without arsenic to obtain the effect of arsenic on the isoelectric point. The experimental isoelectric points decrease from 9.4 (no arsenic and 0.01 mM As) to 6.5 (1 mM As). Using the extended triple-layer model, the isoelectric point is also predicted to decrease, but from 9.4 to 2.3. Although too large, the calculated shift is in qualitative agreement with the direction of the experimental results. The calculated shifts can be sensitive to trace amounts of surface arsenic species not included amongst the three species used in the present study. More extensive sets of adsorption and electrokinetic data would be needed to calibrate more accurate calculation of the electrokinetic results.

The predicted model speciation of arsenate on the surface of am·AlO is given in Fig. 9b–d for $I = 0.01$ and $I = 1.0$ for 4 g $L^{-1}$ as well as $I = 1.0$ for 0.5 g $L^{-1}$ from Fig. 9a. It can be seen in Fig. 9b–d that the bidentate-binuclear species dominates for all pH values less than about 10. It is noteworthy that the monodentate species appears to be much less important compared with iron oxides.

### 3.5. Adsorption of arsenate on β-Al(OH)$_3$ from Arai et al. (2001)

The adsorption data depicted in Fig. 10a refer to arsenate adsorption envelopes on β-Al(OH)$_3$ (Arai et al., 2001). The limited amount of data in Fig. 10a can be fit using only the deprotonated bidentate-binuclear species in

Table 3
Predicted equilibrium constants (referring to site-occupancy standard states) for arsenate adsorption on oxides consistent with the extended triple-layer model[a]:

$\log K^{\theta}_{>SOAsO_3^{2-}}$ : $> SOH_2^+ + H_3AsO_4 => SOAsO_3^{2-} + 3H^+ + H_2O$

$\log K^{\theta}_{(>SO)_2AsO_2^-}$ : $2 > SOH_2^+ + H_3AsO_4 = (> SO)_2AsO_2^- + 3H^+ + 2H_2O$

$\log K^{\theta}_{(>SO)_2AsOOH}$ : $2 > SOH_2^+ + H_3AsO_4 = (> SO)_2AsOOH + 2H^+ + 2H_2O$

| Solid | $\varepsilon_s$[b] | $\log K^{\theta}_{>SOAsO_4^{2-}}$ | $\log K^{\theta}_{(>SO)_2AsO_2^-}$ | $\log K^{\theta}_{(>SO)_2AsOOH}$ |
|---|---|---|---|---|
| $Fe_3O_4$ | 1000 | 1.0 | 5.4 | 6.8 |
| HFO | 1000 | 1.0 | 5.4 | 6.8 |
| α-$MnO_2$ | 1000 | 1.0 | 5.4 | 6.8 |
| α-$TiO_2$ | 121 | 0.36 | 4.8 | 6.4 |
| Ferrihydrite | 32 | −1.5 | 3.2 | 5.2 |
| am.FeO | 32 | −1.5 | 3.2 | 5.2 |
| β-$TiO_2$ | 18.6 | −3.3 | 1.7 | 4.0 |
| FeOOH | 15 | −4.3 | 0.81 | 3.4 |
| $Fe_2O_3$ | 12 | −5.7 | −0.33 | 2.5 |
| α-$Al_2O_3$ | 10.4 | −6.7 | −1.2 | 1.9 |
| γ-$Al_2O_3$ | 10.4 | −6.7 | −1.2 | 1.9 |
| am·AlO | 10.3 | −6.8 | −1.2 | 1.9 |
| β-$Al(OH)_3$ | 10.3 | −6.8 | −1.2 | 1.9 |
| α-$Al(OH)_3$ | 8.4 | −8.5 | −2.8 | 0.66 |
| α-$SiO_2$ | 4.6 | −16.5 | −9.6 | −4.5 |
| am·$SiO_2$ | 3.8 | −20.0 | −12.6 | −6.7 |

[a] Calculated with Eqs. (33)–(35) and the dielectric constants tabulated.
[b] Dielectric constant of the solid from Sverjensky and Fukushi (2006b).

Fig. 1. The other species were included in the model solely to place upper limits on their importance under the experimental conditions studied by Arai et al. (2001). Consequently, the values of $\log K^{\theta}_{(>SO)_2AsOOH}$ and $\log K^{\theta}_{>SOAsO_3^{2-}}$ in Table 2 merely represent upper limits. Arai et al. (2001) also measured a decrease of the isoelectric point with increasing arsenate concentrations from electrophoretic mobility studies. The ETLM prediction again agrees with the direction of the shift, although the overall predicted shift is too large.

The predicted model speciation for arsenate on the surface of β-$Al(OH)_3$ is given in Fig. 10b and c for the lowest and highest ionic strength of Fig. 10a as well as a prediction of the surface speciation at a lower arsenate loading (0.07 mM of arsenate) in Fig. 10d. It can be seen that the bidentate-binuclear species is predicted to dominate in any of these conditions regardless of the pH and ionic strength. These predictions of surface speciation are consistent with the EXAFS and XANES spectroscopic results on the same sample (Arai et al., 2001), which showed only the bidentate-binuclear species regardless of pH and ionic strength. Our predictions in Fig. 10d for even lower surface coverages than those investigated by Arai et al. (2001) indicate that the mononuclear species would become important only at very high pH values (e.g. >10), even when the surface coverages are very low. This is again a significant difference to the results discussed above for the iron oxides.

### 3.6. Adsorption of arsenate on α-$Al(OH)_3$ from Manning and Goldberg (1996)

The data depicted in Fig. 11a show two arsenate adsorption envelopes on α-$Al(OH)_3$ as a function of pH. The solid curves in Fig. 11a represent regression calculations using the three species in Fig. 1 and a site density of 3.0 sites $nm^{-2}$ derived from work on arsenite adsorption on gibbsite (Sverjensky and Fukushi, 2006b). With the exception of data at the highest pH values, the calculated curves provide a close description of the arsenate adsorption over a wide range of conditions shown in Fig. 11a.

The predicted model speciation of arsenate on the surface of α-$Al(OH)_3$ is given in Fig. 11b–d. The surface coverages from Fig. 11a are shown in Fig. 11b and c, and a prediction of the surface speciation in lower ionic strength solutions (0.01 M NaCl) is shown in Fig. 11d. It can be seen in Fig. 11b–d that the bidentate-binuclear species predominates at pH values up to about 10. The predicted surface speciation at low pH is consistent with an EXAFS study of arsenate on α-$Al(OH)_3$ at pH 5.5, which inferred an inner-sphere bidentate-binuclear species (Ladeira et al., 2001). As in Figs. 9 and 10, the mononuclear species is predicted to occur only at the highest pH values, and is little influenced by ionic strength (cf. Fig. 11c and d).

### 3.7. Adsorption of arsenate on α-$Al_2O_3$ from Halter and Pfeifer (2001)

The data depicted in Fig. 12a and b show proton surface titration without arsenate as well as arsenate adsorption envelopes on α-$Al_2O_3$ as functions of pH and surface coverage. The solid curves in Fig. 12a represent regression of the data shown in order to generate values of the electrolyte adsorption equilibrium constants (Table 1). The solid curves in Fig. 12b represent regression calculations using the three reactions in Fig. 1 and a site density of 3.0

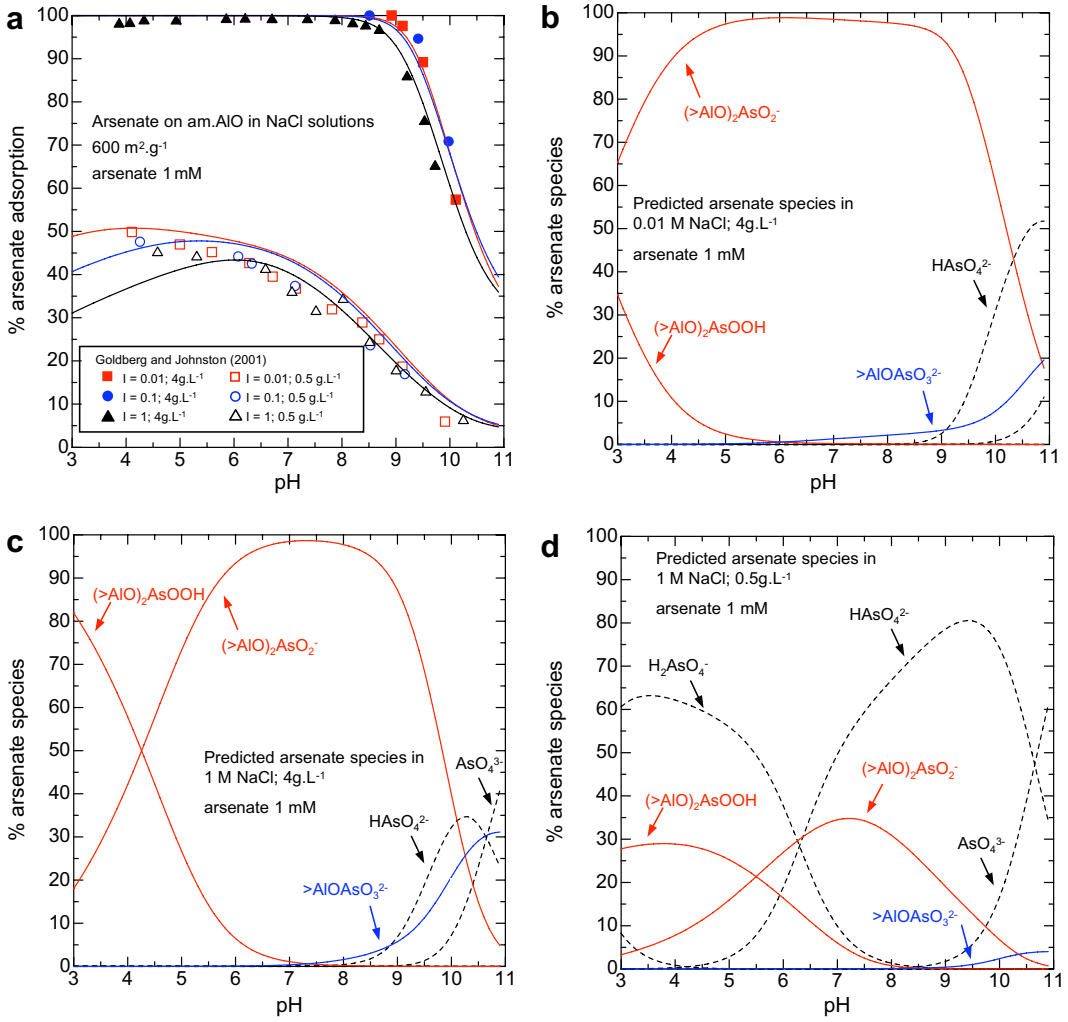


Fig. 9. The data points represent experimental results for arsenate adsorption on am·AlO from Goldberg and Johnston (2001). The solid curves in (a) represent regression calculations with the ETLM using the arsenate surface species and parameters in Tables 1 and 2. (a) Arsenate adsorption as a function of pH, ionic strength and surface coverage. (b–d) Predicted model arsenate surface and aqueous speciation.

sites $nm^{-2}$ derived from work in progress on oxalate adsorption on corundum which refers to a very wide range of surface coverages. This site density is reasonable for singly-coordinated oxygens on corundum. For example, the abundance of such oxygens that can participate in bidentate-binuclear surface complexes varies from 0 to 3.3–8.2 sites $nm^{-2}$ on the (0001), (10–10) and (01–12) faces, respectively. The calculated curves show excellent agreement with the experimental data over a wide range of pH values and the surface coverages shown in Fig. 12b.

The predicted model speciation of arsenate on the surface of $\alpha$-$Al_2O_3$ is given in Fig. 12c–e for the high and low surface coverage of Fig. 12b, as well as a prediction of the surface speciation in solutions with higher arsenate (0.133 mM) to give the same surface coverage as in Fig. 11c for gibbsite. It can be seen in Fig. 12c–e that the bidentate-binculear species dominates at pH values less than about 8–9 and that the mononuclear species contributes substantially to adsorption above these pH values. In this regard, the relative importance of the mononuclear species appears to be greater on corundum than on the other aluminas discussed above. However, when comparing the same surface coverage on corundum (Fig. 12e) with that for gibbsite (Fig. 11c), it can be seen that the arsenate surface speciation on the two aluminas is quite similar.

The predicted dominance of the bidentate-binuclear species at low pH values in Fig. 12c–e is consistent with resonant anomalous X-ray reflectivity (RAXR) studies of arsenate adsorption at pH 5 on the (012) surface of corundum which also established a bidentate-binuclear type of species (Catalano et al., 2006a,b). If the current calculations can be extrapolated to single crystal surfaces, the results of the present study suggest that at high pH values the (012) surface of corundum should show a transition from predominantly binuclear to mononuclear arsenate surface species (see below).

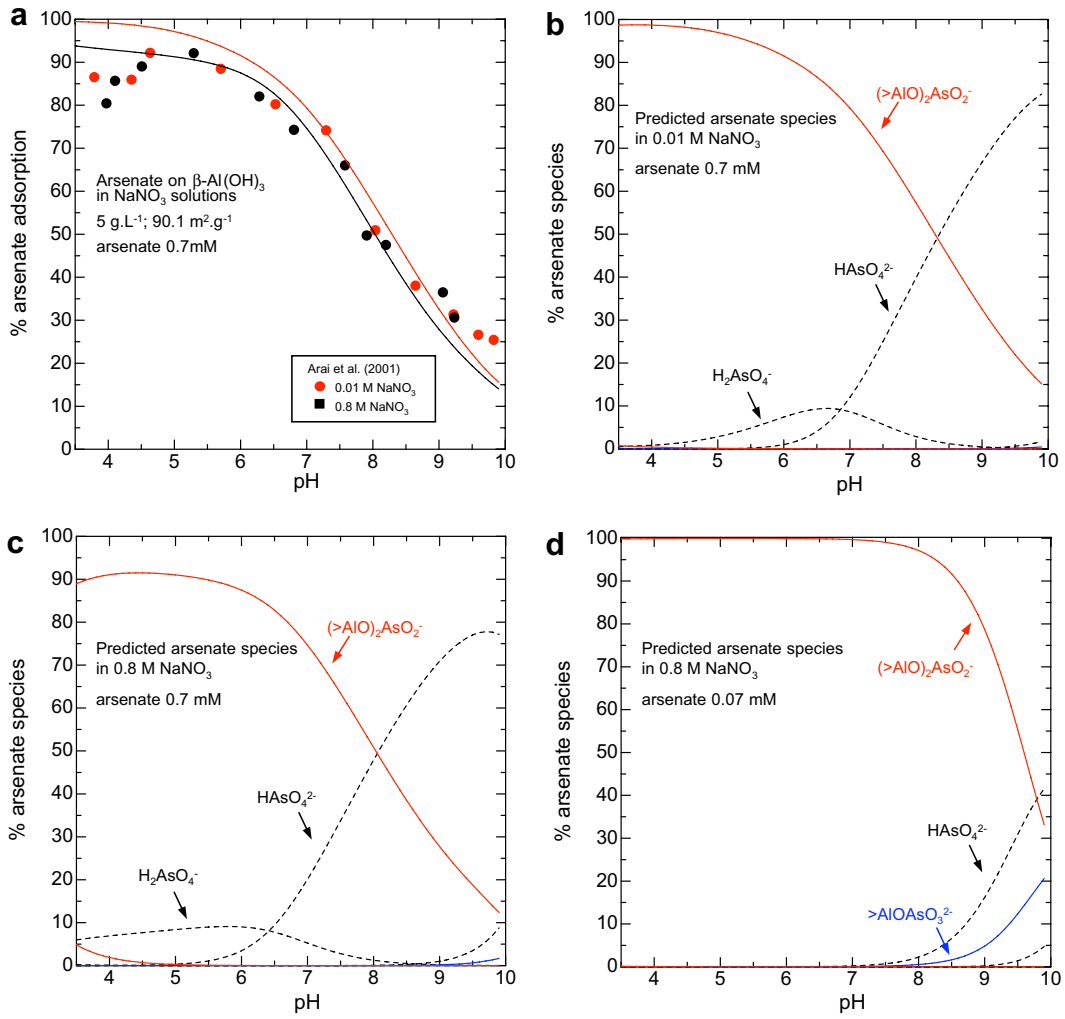


Fig. 10. The data points represent experimental results for arsenate adsorption on β-Al(OH)$_3$ from Arai et al. (2001). The solid curves in (a) represent regression calculations with the ETLM using the arsenate surface species and parameters in Table 1 and 2. (a) Arsenate adsorption as a function of pH and ionic strength. (b–d) Predicted model arsenate surface and aqueous speciation. The bidentate-binuclear species dominates in any experimental conditions regardless of pH and ionic strength consistent with *in situ* X-ray results (Arai et al., 2001).

## 4. PREDICTION OF EQUILIBRIUM CONSTANTS FOR ARSENATE ADSORPTION

### 4.1. Prediction of arsenate adsorption on all oxides

The ETLM calculations summarized above have shown that the three reactions producing the species $(>SO)_2AsO_2^-$, $(>SO)_2AsOOH$ and $>SOAsO_3^{2-}$ (Fig. 1), can describe a variety of arsenate adsorption data including adsorption envelopes, proton coadsorption, and proton titration with arsenic for a very wide range of pH, ionic strength, surface coverage and types of oxides. The equilibrium constants of the arsenate surface species for each oxide retrieved from the regression calculations are summarized in Table 2. In order to compare the equilibrium constants for adsorption on different solids, it is essential to use site-occupancy standard states (i.e. log $K_j^{\theta}$). On this basis, it can be seen in Table 2 that the strength of adsorption of arsenate on oxide surfaces depends strongly on the nature of the solid. An understanding of the systematic differences in the equilibrium constants from one solid to another permits prediction of the adsorption equilibrium constants on all oxides (Sverjensky, 2005, 2006; Sverjensky and Fukushi, 2006).

According to theoretical studies of proton, electrolyte cation and anion, divalent metal ion, and arsenite adsorption (James and Healy, 1972; Sverjensky and Sahai, 1996; Sahai and Sverjensky, 1997; Sverjensky, 2005, 2006; Sverjensky and Fukushi, 2006), the solvation free energy associated with the removal of water molecules from an adsorbing ion opposes the adsorption process and varies from one solid to another. It should be noted that ligand exchange processes during arsenate adsorption also result in release of water as shown in Fig. 1. However, it is assumed that the release of this water is distinct from the release of waters of solvation associated with the adsorbing ions which is the issue under consideration here.

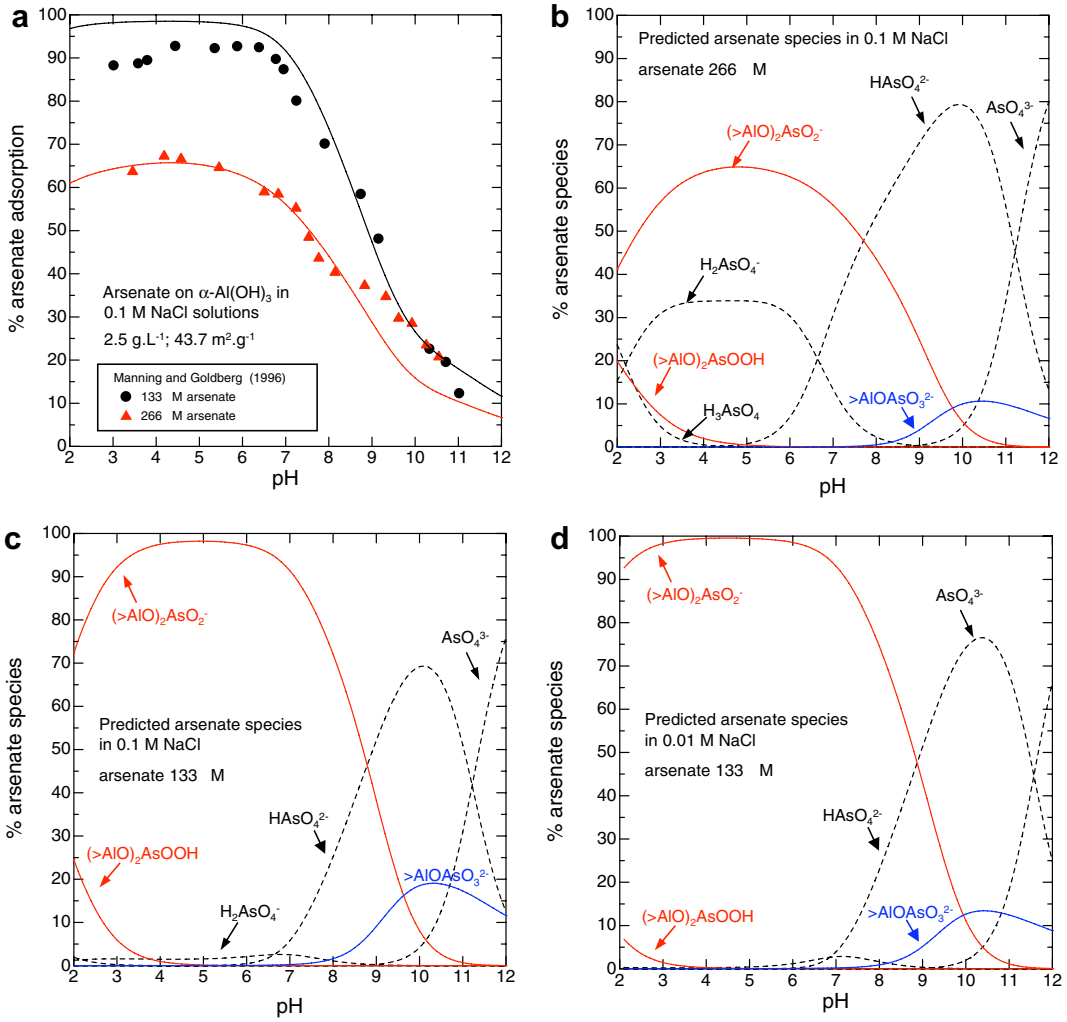


Fig. 11. The data points represent experimental results for arsenate adsorption on α-$Al(OH)_3$ from Manning and Goldberg (1996). The solid curves in (a) represent regression calculations with the ETLM using the arsenate surface species and parameters in Tables 1 and 2. (a) Arsenate adsorption as a function of pH and surface coverage. (b–d) Predicted model arsenate surface and aqueous speciation.

In the present study, we assume that the overall equilibrium constant for adsorption forming the $j$th arsenate surface species ($\log K^{\theta}_{j}$) can be expressed by (Sverjensky and Fukushi, 2006b)

$$\log K^{\theta}_{j} = \frac{-\Delta\Omega_{r,j}}{2.303RT}\left(\frac{1}{\varepsilon_s}\right) + \log K''_{ii,j} \qquad (32)$$

In Eq. (32), the first term on the right-hand side contains $\Delta\Omega_{r,j}$, which represents a Born solvation coefficient for the reaction forming the $j$th species, and $\varepsilon_s$, which represents the dielectric constant of the $s$th solid. The second term, $\log K''_{ii,j}$, represents an intrinsic binding of arsenate independent of the type of oxide. It is assumed here that $\log K''_{ii,j}$ is a constant for a given reaction. The values of $\varepsilon_s$ used in the present study are summarized in Table 2.

Using Eq. (32), we regressed selected values of $\log K^{\theta}_{(>SO)_2AsO_2^-}$, $\log K^{\theta}_{(>SO)_2AsOOH}$ and $\log K^{\theta}_{>SOAsO_3^{2-}}$ from Table 2 as a function of $\frac{1}{\varepsilon_s}$. For goethite, we included only the model goethite from the study by Dixit and Hering (2003) because it has a calculated arsenate surface speciation as a function of pH, ionic strength and surface coverage consistent with trends established in spectroscopic studies for numerous other goethites as discussed above. The regression calculations provide a test of the consistency of the equilibrium constants for our model goethite with those derived for other solids. A further test of this is discussed below. We also did not include the equilibrium constants for the amorphous aluminum oxide derived from the data of Goldberg and Johnston (2001) because these scatter widely relative to the other solids. Finally, because of the similarity in surface speciation of corundum and gibbsite, we assumed that the powdered corundum is probably coated with a gibbsite-like layer and we plotted the corundum equilibrium constants at the value of $\frac{1}{\varepsilon_s}$ for gibbsite. The regression calculations resulted in the lines of best fit shown in Fig. 13a–c and are consistent with the equations

$$\log K^{\theta}_{(>SO)_2AsO_2^-} = -68.5\left(\frac{1}{\varepsilon}\right) + 5.40 \qquad (33)$$

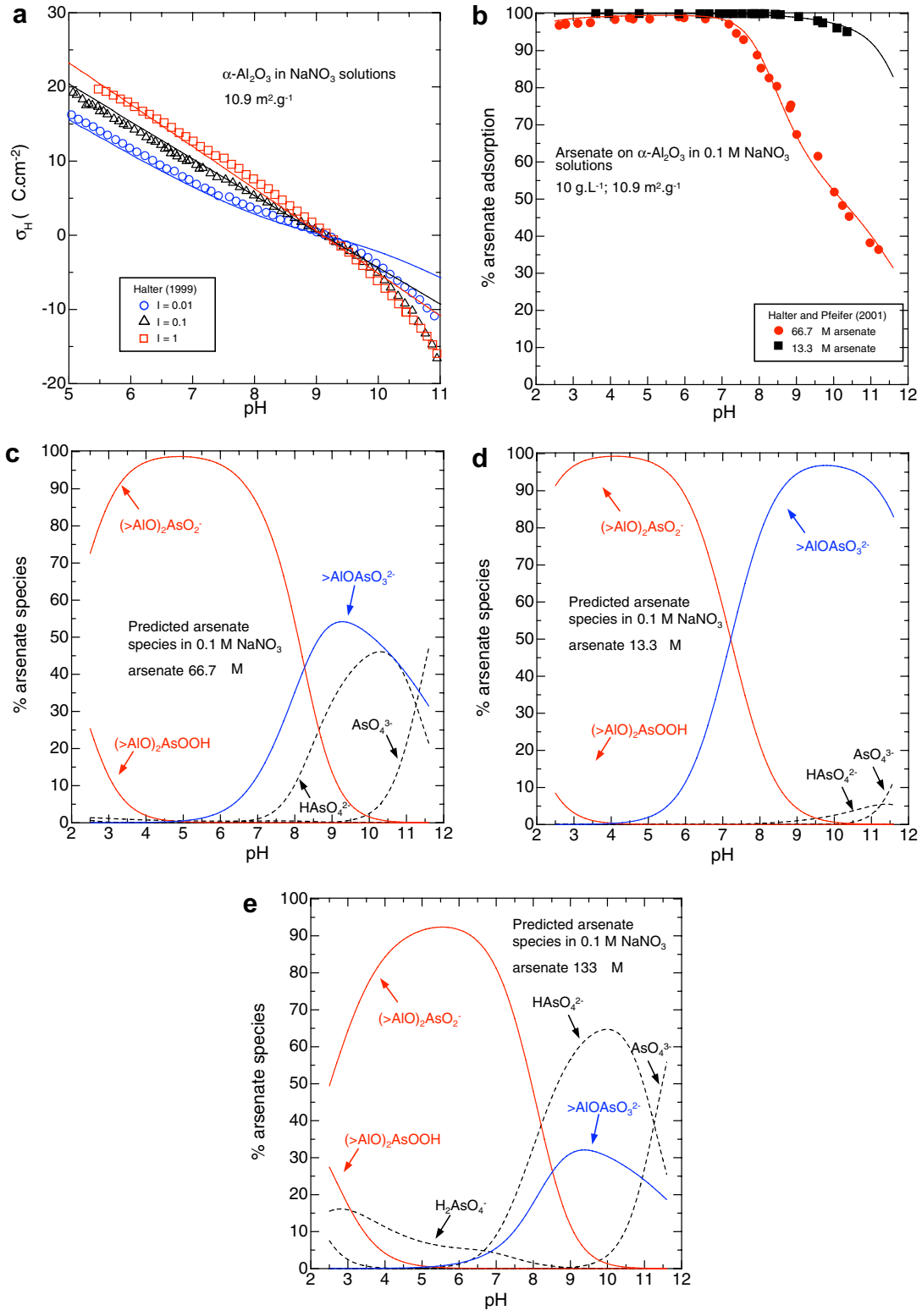


Fig. 12. The data points represent experimental results for proton surface titration and arsenate adsorption on α-$Al_2O_3$ from Halter (1999) and Halter and Pfeifer (2001). The solid curves in (a) and (b) represent regression calculations with the ETLM using the arsenate surface species and parameters in Tables 1 and 2. (a) Proton surface charge on α-$Al_2O_3$ in the absence of arsenate. (b) Arsenate adsorption as a function of pH and surface coverage. (c,d) Predicted model arsenate surface and aqueous speciation for the surface coverages in (b). (e) Predicted arsenate surface and aqueous speciation on α-$Al_2O_3$ to be compared with α-$Al(OH)_3$ at the same surface coverage and ionic strength shown in Fig. 11c.

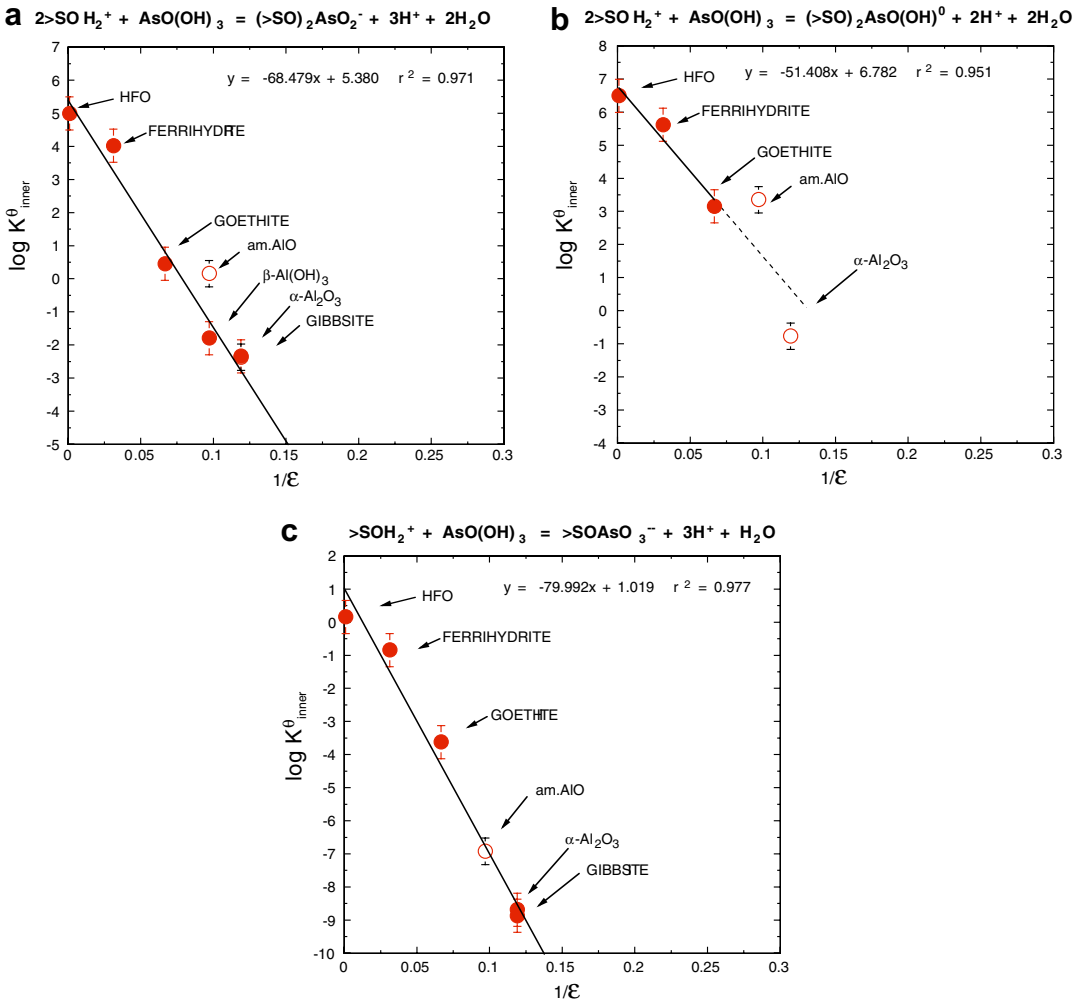


Fig. 13. Correlation of the logarithms of the equilibrium constants for arsenate adsorption on oxides with the inverse of the dielectric constant of the oxide according to Born solvation theory (Table 2). The equilibrium constants represented by the symbols were obtained by analysis of the data in Figs. 2–12 and corrected to be consistent with site-occupancy standard states. The error bars represent uncertainties of ±0.5. The solid symbols were included in the regression, the open symbols were not. The symbol labelled goethite represents equilibrium constants obtained by analysis of the arsenate adsorption data for the goethite from Dixit and Hering (2003) selected as a model goethite based on its surface speciation (see text). The lines were generated by regression with Eqs. (33)–(35).

$$\log K^{\theta}_{(>SO)_2AsOOH} = -51.4\left(\frac{1}{\varepsilon}\right) + 6.78 \quad (34)$$

$$\log K^{\theta}_{>SOAsO_3^{2-}} = -80.0\left(\frac{1}{\varepsilon}\right) + 1.02 \quad (35)$$

It should be noted that the values of $\log K^{\theta}$ for arsenate adsorption in Fig. 13 can be directly compared because they refer to site-occupancy standard states and have been corrected for differences in the $pH_{ZPC}$ as well as site-density and surface area. It is difficult to assess the overall uncertainties in the equilibrium constants because they include uncertainties from regression of the experimental data (about ±0.2 in the $\log K$values) as well as those from the parameters in Eqs. (29)–(31). It is estimated that the uncertainties in the $\log K^{\theta}$ values may be ±0.5 units. It can be seen in Fig. 13a–c that 11 out of the 14 solid symbols represent data points that are within plus or minus 0.5 of the regression lines. Overall, the correlations in Fig. 13 provide a reasonable first order description of the major differences in arsenate adsorption equilibrium constants for a wide range of oxide types. Because Eqs. (33)–(35) have a theoretical basis, they can be used to predict the values of $\log K^{\theta}_{(>SO)_2AsO_2^-}$, $\log K^{\theta}_{(>SO)_2AsOOH}$ and $\log K^{\theta}_{>SOAsO_3^{2-}}$ for other oxides (Table 3).

It is noteworthy that the equilibrium constants for the model goethite (from Dixit and Hering, 2003) plot close to the solid regression lines in Fig. 13a–c. This indicates that the model goethite equilibrium constants are consistent with those of the other solids represented by solid symbols in the figures. In turn, this result supports our selection of this particular goethite as a model goethite for arsenate surface speciation. Additional support can be derived from a prediction of proton coadsorption for a goethite not used in the above analysis of experimental data. For example, using the predicted arsenate equilibrium constants in Table 3 which are consistent with the solid lines in Fig. 13a–c, we

can predict arsenate surface speciation for a goethite under the following conditions: 96 $m^{-2}.g^{-1}$, 10 $g.L^{-1}$, $pH_{ZPC}$ = 9.4, 0.01 $NaNO_3$ solution, pH 6.1 (Rietra et al., 1999). Under these conditions, we predict that the deprotonated bidentate-binuclear arsenate species is dominant relative to the mononuclear complex, which is consistent with the slope of the proton coadsorption data and the interpretation of Rietra et al. (2001). In fact, at the highest surface loading of 0.6 μmol $m^{-2}$ our predicted value of the proton coadsorption is within 20% of the experimental value (for which an uncertainty is not given). Considering the uncertainties already cited above for the predictive correlations, this agreement is quite good. It supports the choice of the Dixit and Hering (2003) goethite as a model goethite for the purposes of the present study and the surface speciation typical of such a goethite, which can be predominantly binuclear at pH values less than neutral and predominantly mononuclear at high pH conditions.

The other three goethites analysed in the present study show a substantial range of values for each equilibrium constant type (Table 2). This is an interesting result given the spectrum of model speciation behavior for goethite discussed above. The range of goethite behavior is puzzling. As noted previously, it may be related to the effect of different crystal faces on different samples (cf. Fig. 6). If true, this raises the possibility that different proportions of crystal faces with very different dielectric constants could produce a scatter in Fig. 13a–c. However, the range of results could also be produced if some of these goethites were contaminated by HFO or magnetite. Clearly further work on goethite surface chemistry will be required to resolve the reason for an apparent range in goethite surface properties. Our selection of the Dixit and Hering (2003) results as a model set of results for goethite is consistent with the results for the other solids investigated here.

It can also be seen in Fig. 13a–c that the differences in the equilibrium constants for HFO, ferrihydite, and goethite are well accounted for by the simple solvation theory expressed by Eq. (32). Even though the dielectric constants of HFO and ferrihydrite should only be regarded as tentative estimates, because they are based on the different $pH_{ZPC}$ values of these solids, they do provide an adequate explanation through Born solvation theory of the substantial differences in the $\log K_j^{\theta}$ values for arsenate adsorption. Higher dielectric constant solids are associated with less work opposing adsorption. A similar result for arsenite adsorption on HFO and ferrihydrite was previously obtained (Sverjensky and Fukushi, 2006b). The results in Fig. 13a–c also indicate that Born solvation theory can explain the stronger adsorption on most iron oxides relative to most aluminum oxides that has been noted in a number of studies (e.g. Kubicki, 2005).

Finally, it can be seen in Fig. 13a–c that the slope of the line for the monodentate-mononuclear complexes is significantly greater than for the two binuclear complexes (cf. Eqs. (33)–(35) above). Clearly the Born solvation effect for mononuclear species is much stronger than for binuclear species. This favors the development of mononuclear species on solids with the highest dielectric constants, such as hydrous ferric oxide, relative to solids with the lowest dielectric constant considered here, such as gibbsite. However, other factors, particularly high pH values and low surface coverages, also strongly favor the mononuclear over the binuclear species as discussed above.

### 4.2. Comparison of arsenate surface speciation on corundum and hematite

A number of studies in the literature have compared ion adsorption on single crystal surfaces of corundum and hematite (Bargar et al., 1997, 2004; Trainor et al., 2001, 2004; Waychunas et al., 2005; Catalano et al., 2006a,b,c,d). Furthermore, MO/DFT calculations (Kubicki, 2005) have indicated a strong preference for arsenate to bind to iron clusters relative to aluminum hydroxide clusters. The general preference of binding of arsenate more strongly to iron oxides relative to aluminum oxides is certainly supported by the calculations and theoretical predictions discussed above. For example, comparison of the speciation and total adsorption of arsenate on HFO relative to goethite in Figs. 7d and 11d, respectively, indicate very different surface speciation, and, at pH values above about 8, a different total amount of adsorption. However, depending on the specific iron and aluminum oxide, the dielectric constants of the two may be sufficiently close that the surface speciation on the two oxides are not as different as in Figs. 7d and 11d.

Even though our study at present does not specifically address single-crystal surfaces, it is interesting to compare the predicted surface speciation for arsenate on corundum and hematite powders, based on the equilibrium constant correlations discussed above. Predicted surface speciation plots for two different surface coverages are shown for corundum and hematite powders in Fig. 14a–d. Clearly, the predicted amounts of adsorption and the surface speciations for the two solids are very similar. For both solids, the binuclear species are predicted to predominate at $pH < 9$ at the higher surface coverage (Fig. 14a and c), and at $pH < 5.5$–6.5 at the lower surface coverage (Fig. 14b and d). However, at pH values higher than these, the mononuclear species is predicted to predominate. This result is a consequence of the stoichiometries of the reactions used for the binuclear versus the mononuclear species. Consequently, on a single crystal surface that has the appropriate spacing of sites such that either binuclear or mononuclear arsenate can adsorb, the results of the present study suggest that the binuclear and the mononuclear will adsorb at different pH values and surface coverages.

The speciation results in Fig. 14 agree qualitatively with the recent single crystal RAXR results for corundum and hematite (0 1 2) surfaces (Catalano et al., 2006a,b), which indicate a bidentate-binuclear surface species at pH 5. EXAFS results for a hematite powder at pH values of 4.5–8.0 and surface coverages of 0.45–3.10 μmol $m^{-2}$ (Arai et al., 2004) also reported a bidentate-binuclear species predominating. However, the latter authors did note a minor amount of a possible bidentate-mononuclear species. It seems possible that this mononuclear species is consistent with the mononuclear species in our speciation calculations

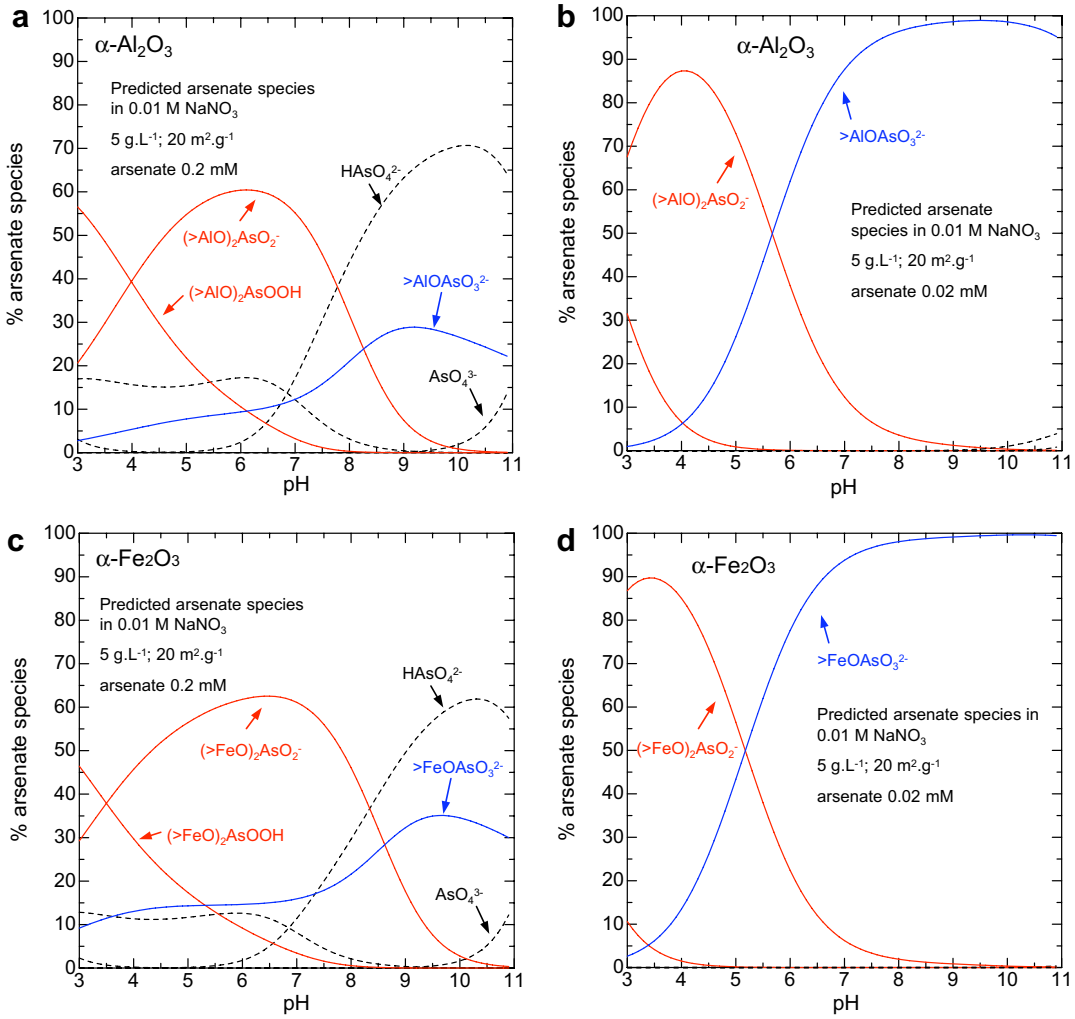


Fig. 14. Predicted arsenate surface speciation on corundum and hematite powders at two different surface coverages. The curves were calculated with the ETLM using the arsenate surface species and predicted equilibrium constants in Table 3 assuming values of the $pH_{ZPC} = 9.4$ and 9.5 for corundum and hematite, respectively. (a) Corundum, 2.0 μmol/m$^2$ of arsenate if 100% adsorbed. (b) Corundum, 0.2 μmol/m$^2$ of arsenate if 100% adsorbed. (c) Hematite, 2.0 μmol/m$^2$ of arsenate if 100% adsorbed. (d) Hematite, 0.2 μmol/m$^2$ of arsenate if 100% adsorbed.

for hematite (e.g. Eq. 20, which has the same reaction stoichiometry as Eq. (14). However, the possible pH and surface coverage dependence of this species was not addressed in the EXAFS study.

## 5. CONCLUSIONS

In the present study, we applied the ETLM to a wide variety of surface chemical measurements for arsenate on oxide surfaces. The main goal of the study was to use evidence from X-ray and infrared spectroscopic and theoretical molecular studies to guide the choice of arsenate surface species and to determine the effects of pH, ionic strength, surface coverage and type of oxide on the surface speciation. A second goal was to place arsenate surface equilibria on a predictive basis. The findings of the present study are as follows:

(1) Three reaction stoichiometries forming inner-sphere arsenate surface species

$$2 > SOH + H_3AsO_4^0 = (> SO)_2AsO_2^- + H^+ + 2H_2O$$
$$2 > SOH + H_3AsO_4^0 = (> SO)_2AsOOH + 2H_2O$$

and

$$> SOH + H_3AsO_4^0 = > SOAsO_3^{2-} + 2H^+ + H_2O$$

were derived from *in situ* X-ray and infrared spectroscopic evidence for arsenate and phosphate adsorption on goethite. These three reaction stoichiometries were found to be consistent with experimental studies of adsorption envelope, proton titration and proton coadsorption with arsenate referring to wide ranges of pH, ionic strength and surface coverage for a variety of solids including goethite, hematite, HFO, ferrihydrite, amorphous aluminum oxide,

β-$Al(OH)_3$, α-$Al(OH)_3$ and α-$Al_2O_3$. Surface coverage limits for adsorption (on goethite) were found to be about 2.5 μmol $m^{-2}$. At higher coverages, sorption processes in addition to adsorption (e.g. precipitation) must be important. The three surface arsenic species used here result in prediction of decreases of the isoelectric point with arsenic loading, although the magnitude of the calculated shift is too large for aluminum oxides. Further experimental data and calculations will be needed to address this issue more accurately.

(2) One goethite sample (from Dixit and Hering, 2003) was elected as a model goethite for arsenate speciation because it shows predicted behavior in which binuclear species predominate at higher surface coverages and lower pH values compared to mononuclear species in agreement with *in situ* FTIR spectroscopic results for phosphate adsorption on one goethite (Tejedor-Tejedor and Anderson, 1990) and EXAFS results for three goethites (Waychunas et al., 1993; Farquhar et al., 2002; and Sherman and Randall, 2003). However, several other goethites studied here show predicted surface speciations of predominantly binuclear (Gao and Mucci, 2001) to predominantly mononuclear (Antelo et al., 2005). Although recent preliminary reports of *in situ* ATR-FTIR results for phosphate and arsenate on goethite (e.g. Loring et al., 2006; Nelson et al., 2006) also indicate mononuclear surface species, and a recent study of phosphate on hematite (Elzinga and Sparks, 2007) indicates the possible existence of species that are partly mononuclear and partly H-bonded, it is clear that much remains to be done to further characterize goethite surface chemistry, including further work on the interpretation of IR spectra, establishing the proportions of different crystal faces on samples used in adsorption studies, the role of carbonate adsorption, and the possibility of surface coatings of amorphous or poorly crystalline iron oxides, all of which could be contributing to the apparent differences in goethite surface speciation indicated above.

(3) The predicted surface speciation of arsenate on HFO, ferrihydrite, hematite, corundum and β-$Al(OH)_3$ showed that bidentate-binuclear species were predominant under conditions consistent with EXAFS results (Waychunas et al., 1993; Arai et al., 2001, 2004) and recent X-ray reflectivity, standing-wave and RAXR studies of single crystal surfaces (Catalano et al., 2006a,b; Catalano et al., 2007).

(4) The equilibrium constants for arsenate adsorption ($\log K^{\theta}_{(>SO)_2AsO_2^-}$, $\log K^{\theta}_{(>SO)_2AsOOH}$ and $\log K^{\theta}_{>SOAsO_3^{2-}}$) in terms of site-occupancy standard states show systematic differences on different solids, including the model goethite from Dixit and Hering (2003). The differences were explained with the aid of Born solvation theory which enabled the development of a set of predictive equations for arsenate adsorption equilibrium constants on all oxides.

(5) The predictive equations indicate that the Born solvation effect for mononuclear species is much stronger than for binuclear species. This favors the development of the mononuclear species on iron oxides with the highest dielectric constant, such as hydrous ferric oxide, relative to aluminum oxides with the lowest dielectric constant, such as gibbsite. On hematite and corundum, which have much closer dielectric constants, the surface speciation of arsenate is predicted to be rather similar, depending on the specific characteristics of the samples. The binuclear species are predicted to predominate at lower pH values and higher surface coverages than the mononuclear species.

## ACKNOWLEDGMENTS

We greatly appreciate discussions with Y. Arai, J. Catalano, J.A. Davis, J. Loring, D.B. Kent, J.D. Kubicki and G.A. Waychunas. We also wish to acknowledge the helpful comments on the manuscript from three reviewers and Associate Editor M. Machesky. Financial support was provided by DuPont Engineering and DOE Grant DE-FG02-96ER-14616.

## REFERENCES

Anderson M. A. and Malotky D. T. (1979) The adsorption of protolyzable anions on hydrous oxides at the isoelectric pH. *J. Colloid Interf. Sci.* **72**, 413–427.

Antelo J., Avena M., Fiol S., Lopez R. and Arce F. (2005) Effects of pH and ionic strength on the adsorption of phosphate and arsenate at the goethite-water interface. *J. Colloid Interf. Sci.* **285**, 476–486.

Arai Y., Elzinga E. and Sparks D. L. (2001) X-ray absorption spectroscopic investigation of arsenite and arsenate adsorption at the aluminum oxide–water interface. *J. Colloid Interf. Sci.* **235**, 80–88.

Arai Y. and Sparks D. L. (2001) ATR-FTIR spectroscopic investigation on phosphate adsorption mechanisms at the ferrihydrite–water interface. *J. Colloid Interf. Sci.* **241**, 317–326.

Arai Y., Sparks D. L. and Davis J. A. (2004) Effects of dissolved carbonate on arsenate adsorption and surface speciation at the hematite-water interface. *Environ. Sci. Technol.* **38**(3), 817–824.

Bargar J. R., Towle S. N., Brown G. E. J. and Parks G. A. (2004) In situ grazing incidence extended X-ray adsorption fine structure study of Pb(II) chemisorption on hematite (0001) and (1–102) surfaces. *Langmuir* **20**, 1667–1673.

Bargar J. R., Towle S. N., Brown G. E. J. and Parks G. A. (1997) XAFS and bond-valence determination of the structures and compositions of surface functional groups and Pb(II) and Co(II) sorption products on single-crystal α-$Al_2O_3$. *J. Colloid Interf. Sci.* **185**, 473–492.

Blesa M. A., Weisz A. D., Morando P. J., Salfity J. A., Magaz G. E. and Regazzoni A. e. (2000) The interaction of metal oxide surfaces with complexing agents dissolved in water. *Coord. Chem. Rev.* **196**, 31–63.

Catalano J. G., Park C., Zhang Z. and Fenter P. (2006a) Simultaneous inner- and outer-sphere As(V) adsorption on iron and aluminum oxide surfaces. *American Geophysical Union, Spring Meeting*.

Catalano J. G., Park C., Zhang Z. and Fenter, P. (2006b) *Simultaneous Inner- and Outer-sphere As(V) Adsorption on α-$Al_2O_3$*. American Chemical Society, 231st Annual Meeting.

Catalano J. G., Park C., Zhang Z. and Fenter P. (2006c) Termination and water adsorption at the α-$Al_2O_3$ (012)–aqueous solution interface. *Langmuir* **22**, 4668–4673.

Catalano J. G., Zhang Z., Fenter P. and Bedzyk M. J. (2006d) Inner-sphere adsorption geometry of Se(IV) at the hematite (100)–water interface. *J. Colloid Interf. Sci.* **297**, 665–671.

Catalano J. G., Zhang Z., Park C., Fenter P. and Bedzyk M. J. (2007) Bridging arsenate surface complexes on the hematite (012) surface. *Geochim. Cosmochim. Acta* **71**, 1883–1897.

Criscenti L. J. and Sverjensky D. A. (1999) The role of electrolyte anions $ClO_4^-$, $NO_3^-$, and $Cl^-$ in divalent metal ($M^{2+}$)

adsorption on oxide and hydroxide surfaces in salt solutions. *Amer. J. Sci.* **299**, 828–899.

Criscenti L. J. and Sverjensky D. A. (2002) A single-site model for divalent and heavy metal adsorption over a range of metal concentrations. *J. Colloid Interf. Sci.* **253**, 329–352.

Davis J. A. and Leckie J. O. (1978) Surface ionization and complexation at the oxide/water interface. II. Surface properties of amorphous iron oxyhydroxide and adsorption of metal ions. *J. Colloid Interf. Sci.* **67**, 90–107.

Dixit S. and Hering J. G. (2003) Comparison of arsenic(V) and arsenic(III) sorption onto iron oxide minerals: Implications for arsenic mobility. *Environ. Sci. Technol.* **37**(18), 4182–4189.

Dutta P. K., Ray A. K., Sharma V. K. and Millero F. J. (2004) Adsorption of arsenate and arsenite on titanium dioxide suspensions. *J. Colloid Interf. Sci.* **278**, 270–275.

Dzombak D. A. and Morel F. M. M. (1990) *Surface Complexation Modeling*. John Wiley and Sons, New York.

Elzinga E. J. and Sparks D. L. (2007) Phosphate adsorption onto hematite: An in situ ATR-FTIR investigation of the effects of pH and loading level on the mode of phosphate surface complexation. *J. Colloid Interf. Sci.* **308**, 53–70.

Farquhar M. L., Charnock J. M., Livens F. R. and Vaughan D. J. (2002) Mechanisms of arsenic uptake from aqueous solution by interaction with goethite, lepidocrocite, mackinawite, and pyrite: an X-ray absorption spectroscopy study. *Environ. Sci. Technol.* **36**(8), 1757–1762.

Fendorf S., Eick M. J., Grossl P. and Sparks D. L. (1997) Arsenate and chromate retention mechanisms on goethite. 1. Surface structure. *Environ. Sci. Technol.* **31**(2), 315–320.

Fukushi K., Sasaki M., Sato T., Yanase N., Amano H. and Ikeda H. (2003) A natural attenuation of arsenic in drainage from an abandoned arsenic mine dump. *Appl. Geochem.* **18**(8), 1267–1278.

Fukushi K. and Sverjensky D. A. (2007) A surface complexation model for sulfate and selenate on iron oxides consistent with spectroscopic and theoretical molecular evidence. *Geochim. Cosmochim. Acta* **71**, 1–24.

Fuller C. C. and Davis J. A. (1989) Influence of coupling of sorption and photosynthetic processes on trace-element cycles in natural-waters. *Nature* **340**(6228), 52–54.

Gaboriaud F. and Ehrhardt J. (2003) Effects of different crystal faces on the surface charge of colloidal goethite (α-FeOOH) particles: an experimental and modeling study. *Geochim. Cosmochim. Acta* **67**, 967–983.

Gao Y. and Mucci A. (2001) Acid base reactions, phosphate and arsenate complexation, and their competitive adsorption at the surface of goethite in 0.7 M NaCl solution. *Geochim. Cosmochim. Acta* **65**(14), 2361–2378.

Gao Y. and Mucci A. (2003) Individual and competitive adsorption of phosphate and arsenate on goethite in artificial seawater. *Chem. Geol.* **199**(1–2), 91–109.

Goldberg S. (1986) Chemical modeling of arsenate adsorption on aluminum and iron-oxide minerals. *Soil Sci. Soc. Am. J.* **50**(5), 1154–1157.

Goldberg S. and Johnston C. T. (2001) Mechanisms of arsenic adsorption on amorphous oxides evaluated using macroscopic measurements, vibrational spectroscopy, and surface complexation modeling. *J. Colloid Interf. Sci.* **234**, 204–216.

Grossl P. R., Eick M., Sparks D. L., Goldberg S. and Ainsworth C. C. (1997) Arsenate and chromate retention mechanisms on goethite. 2. Kinetic evaluation using a pressure-jump relaxation technique. *Environ. Sci. Technol.* **31**(2), 321–326.

Halter W. E. (1999) Surface acidity constants of alpha-$Al_2O_3$ between 25 and 70 °C. *Geochim. Cosmochim. Acta* **63**, 3077–3085.

Halter W. E. and Pfeifer H. R. (2001) Arsenic(V) adsorption onto alpha-$Al_2O_3$ between 25 and 70 degrees C. *Appl. Geochem.* **16**(7–8), 793–802.

Hayes K. F., Papelis C. and Leckie J. O. (1988) Modeling ionic strength effects on anion adsorption at hydrous oxide/solution interfaces. *J. Colloid Interf. Sci.* **125**, 717–726.

Helgeson H. C., Kirkham D. H. and Flowers G. C. (1981) Theoretical prediction of the thermodynamic behavior of aqueous electrolytes at high pressures and temperatures. IV. Calculation of activity coefficients, osmotic coefficients, and apparent molal and standard and relative partial molal properties to 5 kb and 600 °C. *Amer. J. Sci.* **281**, 1241–1516.

Hering J. G. and Dixit S. (2005) Contrasting sorption behavior of arsenic(III) and arsenic(V) in suspensions of iron and aluminum oxyhydroxides. *Adv. Arsenic Res.* **915**, 8–24.

Hiemstra T. and van Riemsdijk W. H. (1999) Surface structural ion adsorption modeling of competitive binding of oxyanions by metal (hydr)oxides. *J. Colloid Interf. Sci.* **210**, 182–193.

Hopenhayn C. (2006) Arsenic in drinking water: impact on human health. *Elements* **2**(2), 103–107.

Jain A. and Loeppert R. H. (2000) Effect of competing anions on the adsorption of arsenate and arsenite by ferrihydrite. *J. Environ. Quality* **29**(5), 1422–1430.

Jain A., Raven K. P. and Loeppert R. H. (1999) Arsenite and arsenate adsorption on ferrihydrite: surface charge reduction and net OH-release stoichiometry. *Environ. Sci. Technol.* **33**(8), 1179–1184.

James R. O. and Healy T. W. (1972) Adsorption of hydrolyzable metal ions at the oxide–water interface. III. A thermodynamic model of adsorption. *J. Colloid Interf. Sci.* **40**, 65–81.

Jia Y., Xu L., Fang Z. and Demopoulos G. P. (2006) Observation of surface precipitation of arsenate on ferrihydrite. *Environ. Sci. Technol.* **40**(10), 3248–3253.

Koretsky C. M., Sverjensky D. A. and Sahai N. (1998) A model of surface site types on oxide and silicate minerals based on crystal chemistry: implications for site types and densities, multi-site adsorption, surface infrared spectroscopy, and dissolution kinetics. *Amer. J. Sci.* **298**, 349–438.

Kubicki J. D. (2005) Comparison of As(III) and As(V) complexation onto Al- and Fe-hydroxides. In *Advances in Arsenic Research: Integration of Experimental and Observational Studies and Implications for Migration*, Vol. 915 (ed. L. Benning). American Chemical Society, Washington, DC, pp. 104–117.

Kwon K. D. and Kubicki J. D. (2004) Molecular orbital theory study on surface complex structures of phosphates to iron hydroxides: Calculation of vibrational frequencies and adsorption energies. *Langmuir* **20**, 9249–9254.

Ladeira A. C. Q., Ciminelli V. S. T., Duarte H. A., Alves M. C. M. and Ramos A. Y. (2001) Mechanism of anion retention from EXAFS and density functional calculations: Arsenic (V) adsorbed on gibbsite. *Geochim. Cosmochim. Acta* **65**(8), 1211–1217.

Loring J. S., Sjoberg S. and Persson P. (2006) *Phosphate Forms Monodentate Complexes at the Surface of Goethite*. American Chemical Society, 232nd Annual Meeting.

Manceau A. (1995) The mechanism of anion adsorption on iron oxides: evidence for the bonding of arsenate tetrahedra on free $Fe(O,OH)_6$ edges. *Geochim. Cosmochim. Acta* **59**, 3647–3653.

Manning B. A. and Goldberg S. (1996) Modeling competitive adsorption of arsenate with phosphate and molybdate on oxide minerals. *Soil Sci. Soc. Am. J.* **60**(1), 121–131.

Manning B. A. and Goldberg S. (1997) Adsorption and stability of arsenic(III) at the clay mineral-water interface. *Environ. Sci. Technol.* **31**(7), 2005–2011.

Myneni S. C. B., Traina S. J., Waychunas G. A. and Logan T. J. (1998) Experimental and theoretical vibrational spectroscopic

evaluation of arsenate coordination in aqueous solutions, solids, and at mineral–water interfaces. *Geochim. Cosmochim. Acta* **62**(19–20), 3285–3300.

Nelson H., Persson P., Lovgren L., Sjoberg S. and Loring J. S. (2006) Arsenate Adsorption to Goethite Studied by Combining Spectroscopy and Potentiometry. American Chemical Society, 232nd Annual Meeting.

Nordstrom D. K. (2002) Public health—Worldwide occurrences of arsenic in ground water. *Science* **296**(5576), 2143–2145.

Nordstrom D. K. and Archer D. G. (2003) Arsenic thermodynamic data and environmental geochemistry. In *Arsenic in Ground Water: Geochemistry and Occurrence* (eds. Welch, A. H. and Stollenwerk, K. G.). Kluwer Academic Publishers, Dordrecht, pp. 1–25.

Pena M. E., Korfiatis G. P., Patel M., Lippincott L. and Meng X. (2005) Adsorption of As(V) and As(III) by nanocrystalline titanium dioxide. *Water Res.* **39**, 2327–2337.

Pena M. E., Meng X., Korfiatis G. P. and Jing C. (2006) Adsorption mechanism of arsenic on nanocrystalline titanium dioxide. *Environ. Sci. Technol.* **40**, 1247–1262.

Persson P., Nilsson N. and Sjoberg S. (1996) Structure and bonding of orthophosphate ions at the iron oxide–aqueous interface. *J. Colloid Interf. Sci.* **177**, 263–275.

Pichler T., Veizer J. and Hall G. E. M. (1999) Natural input of arsenic into a coral reef ecosystem by hydrothermal fluids and its removal by Fe(III) oxyhydroxides. *Environ. Sci. Technol.* **33**(9), 1373–1378.

Prélot B., Villiéras F., Pelletier M., Gérard G., Gaboriaud F., Ehrhardt J. J., Perrone J., Fedoroff M., Jeanjean J., Lefevre G., Mazrolles M., Pastol J., Rouchaud J. and Lindecker C. (2003) Morphology and surface heterogeneities in synthetic goethites. *J. Colloid Interf. Sci.* **261**, 244–254.

Raven K. P., Jain A. and Loeppert R. H. (1998) Arsenite and arsenate adsorption on ferrihydrite: kinetics, equilibrium, and adsorption envelopes. *Environ. Sci. Technol.* **32**(3), 344–349.

Rietra R. P. J. J., Hiemstra T. and van Riemsdijk W. H. (1999) The relationship between molecular structure and ion adsorption on variable charge minerals. *Geochim. Cosmochim. Acta* **63**, 3009–3015.

Rietra R. P. J. J., Hiemstra T. and van Riemsdijk W. H. (2001) Comparison of selenate and sulfate adsorption on goethite. *J. Colloid Interf. Sci.* **240**, 384–390.

Roddick-Lanzilotta A. J., McQuillan A. J. and Craw D. (2002) Infrared spectroscopic characterisation of arsenate (V) ion adsorption from mine waters, Macraes mine, New Zealand. *Appl. Geochem.* **17**(4), 445–454.

Sahai N. and Sverjensky D. A. (1997) Solvation and electrostatic model for specific electrolyte adsorption. *Geochim. Cosmochim. Acta* **61**, 2827–2848.

Sahai N. and Sverjensky D. A. (1998) GEOSURF: a computer program for forward modeling of adsorption on mineral surfaces in aqueous solution. *Comput. Geosci.* **24**, 853–873.

Sherman D. M. and Randall S. R. (2003) Surface complexation of arsenic(V) to iron(III) (hydr)oxides: structural mechanism from ab initio molecular geometries and EXAFS spectroscopy. *Geochim. Cosmochim. Acta* **67**(22), 4223.

Stanforth R. (1999) Comment on "Arsenite and arsenate adsorption on ferrihydrate: surface charge reduction and net OH-release stoichiometry". *Environ. Sci. Technol.* **33**(20), 3695.

Suarez D. L., Goldberg S., Su C. and Manning B. A. (1997) Evaluation of oxyanion adsorption mechanisms on oxides using FTIR spectroscopy and electrophoretic mobility. *Abstr. Papers Amer. Chem. Soc.* **213**, 59-GEOC.

Sun X. and Doner H. E. (1996) An investigation of arsenate and arsenite bonding structures on goethite by FTIR. *Soil Sci.* **161**, 865–872.

Sverjensky D. A. (2003) Standard states for the activities of mineral surface-sites and species. *Geochim. Cosmochim. Acta* **67**, 17–28.

Sverjensky D. A. (2005) Prediction of surface charge on oxides in salt solutions: Revisions for 1:1 (M + L−) electrolytes. *Geochim. Cosmochim. Acta* **69**(2), 225.

Sverjensky D. A. (2006) Prediction of the speciation of alkaline earths adsorbed on mineral surfaces in salt solutions. *Geochim. Cosmochim. Acta* **70**(10), 2427–2453.

Sverjensky D. A. and Fukushi K. (2006a) Anion adsorption on oxide surfaces: inclusion of the water dipole in modeling the electrostatics of ligand exchange. *Environ. Sci. Technol.* **40**, 263–271.

Sverjensky D. A. and Fukushi K. (2006b) A predictive model (ETLM) for As(III) adsorption and surface speciation on oxides consistent with spectroscopic data. *Geochim. Cosmochim. Acta* **70**, 3778–3802.

Sverjensky D. A. and Sahai N. (1996) Theoretical prediction of single-site surface protonation equilibrium constants for oxides and silicates in water. *Geochim. Cosmochim. Acta* **60**, 3773–3798.

Tejedor-Tejedor M. I. and Anderson M. A. (1990) Protonation of phosphate on the surface of goethite as studied by CIR-FTIR and electrophoretic mobility. *Langmuir* **6**(3), 602–611.

Trainor T. P., Chaka A. M., Eng P. J., Newville M., Waychunas G. A., Catalano J. G. and Brown G. E. J. (2004) Structure and reactivity of the hydrated hematite (0 0 0 1) surface. *Surf. Sci.* **573**, 204–224.

Trainor T. P., Fitts J. P., Templeton A. S., Grolimund D. and Brown G. E. J. (2001) Grazing incidence XAFS study of aqueous Zn(II) sorption on $\alpha$-$Al_2O_3$ single crystals. *J. Colloid Interf. Sci.* **244**, 239–244.

Villalobos M., Trotz M. A. and Leckie J. O. (2003) Variability in goethite surface site density: evidence from proton and carbonate adsorption. *J. Colloid Interf. Sci.* **268**, 273–287.

Voegelin A. and Hug S. J. (2003) Catalyzed oxidation of arsenic(III) by hydrogen peroxide on the surface of ferrihydrite: an in situ ATR-FTIR study. *Environ. Sci. Technol.* **37**(5), 972–978.

Waychunas G. A., Rea B. A., Fuller C. C. and Davis J. A. (1993) Surface chemistry of ferrihydrite. 1. EXAFS studies of the geometry of coprecipitated and adsorbed arsenate. *Geochim. Cosmochim. Acta* **57**(10), 2251–2269.

Waychunas G. A., Trainor T. P., Eng P. J., Catalano J. G., Brown, Jr., G. R., Davis J., Rogers J. and Bargar J. (2005) Surface complexation studied via combined grazing-incidence EXAFS and surface diffraction: arsenate on hematite (0 0 0 1) and (1–12). *Anal. Bioanal. Chem.* **383**, 12–27.

Weidler P. G., Schwinn T. and Gaub H. E. (1996) Vicinal faces on synthetic goethite observed by atomic force microscopy. *Clay. Clay Miner.* **44**, 437–442.

Yoon T. H., Johnson S. B., Musgrave C. B. and Brown, Jr., G. E. (2004) Adsorption of organic matter at mineral/water interfaces: I. ATR-FTIR spectroscopic and quantum chemical study of oxalate adsorbed at boehmite/water and corundum/water interfaces. *Geochim. Cosmochim. Acta* **68**, 4505–4518.

Zhang J. S. and Stanforth R. (2005) Slow adsorption reaction between arsenic species and goethite (alpha-FeOOH): diffusion or heterogeneous surface reaction control. *Langmuir* **21**(7), 2895–2901.

*Associate editor:* Michael L. Machesky